

RE-ENGINEERING REDOX-SENSITIVE GREEN FLUORESCENT PROTEIN AS  
INDICATORS OF CELLULAR THIOL OXIDATION STATUS

by

MARK BRIMHALL CANNON

A DISSERTATION

Presented to the Department of Chemistry  
and the Graduate School of the University of Oregon  
in partial fulfillment of the requirements  
for the degree of  
Doctor of Philosophy

June 2005

UMI Number: 3181089

## INFORMATION TO USERS

The quality of this reproduction is dependent upon the quality of the copy submitted. Broken or indistinct print, colored or poor quality illustrations and photographs, print bleed-through, substandard margins, and improper alignment can adversely affect reproduction.

In the unlikely event that the author did not send a complete manuscript and there are missing pages, these will be noted. Also, if unauthorized copyright material had to be removed, a note will indicate the deletion.

**UMI<sup>®</sup>**

---

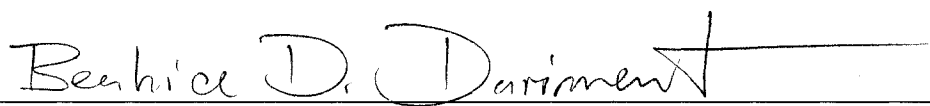
UMI Microform 3181089

Copyright 2005 by ProQuest Information and Learning Company.

All rights reserved. This microform edition is protected against unauthorized copying under Title 17, United States Code.

ProQuest Information and Learning Company  
300 North Zeeb Road  
P.O. Box 1346  
Ann Arbor, MI 48106-1346


“Re-engineering Redox-Sensitive Green Fluorescent Protein as Indicators of Cellular Thiol Oxidation Status,” a dissertation prepared by Mark Brimhall Cannon in partial fulfillment of the requirements for the Doctor of Philosophy degree in the Department of Chemistry. This dissertation has been approved and accepted by:

  
\_\_\_\_\_  
Dr. Beatrice Darimont, Chair of the Examining Committee

05-31-05  
\_\_\_\_\_  
Date

Committee in Charge:      Dr. Beatrice Darimont, Chair  
                                     Dr. S. James Remington, Advisor  
                                     Dr. Brian W. Matthews  
                                     Dr. Bruce P. Branchaud  
                                     Dr. Diane Hawley

Accepted by:

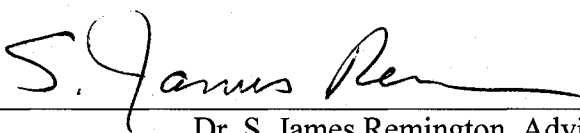
  
\_\_\_\_\_  
Dean of the Graduate School

© 2005 Mark Brimhall Cannon

## An Abstract of the Dissertation of

Mark Brimhall Cannon                      for the degree of                      Doctor of Philosophy  
in the Department of Chemistry                      to be taken                      June 2005

Title: RE-ENGINEERING REDOX-SENSITIVE GREEN FLUORESCENT PROTEIN  
AS INDICATORS OF CELLULAR THIOL OXIDATION STATUS

Approved:  \_\_\_\_\_  
Dr. S. James Remington, Advisor

The oxidation state of thiols has a crucial role in the regulation of many cellular processes. As an allosteric control mechanism, the oxidation state of protein thiols rivals that of protein phosphorylation. Unfortunately, conventional methods for determination of cellular thiol oxidation status are cumbersome, invasive and do not permit high spatial and temporal resolution of transient events.

Redox-sensitive variants of the green fluorescent protein (designated roGFPs) have been developed that allow “real-time” monitoring of the redox status of cellular compartments by ratiometric changes in fluorescence excitation. However, the slow response time of these probes will limit the study of many interesting redox processes, such as H<sub>2</sub>O<sub>2</sub> bursts in cell signaling.

In order to improve response time for these indicators up to three positively charged amino acids have been substituted at positions adjacent to the disulfide in

roGFP1 by site-directed mutagenesis. The disulfide midpoint potentials and pseudo-first order rate constants for oxidation by  $\text{H}_2\text{O}_2$  and reduction by DTT were determined for these mutants (designated roGFP1-R1 through R14). In accord with simple electrostatic considerations, the rate constants increase with each additional positively-charged substitution placed near the disulfide, up to almost an order of magnitude increase in rate. The midpoint potentials, in general, become more oxidizing with increasing numbers of positive substitutions.

The crystal structures of two of these variants with opposite disulfide oxidation states have been determined: a 2.2 Å resolution oxidized structure of the “R7” mutant with two basic substitutions, and a 1.95 Å resolution reduced structure of the “R8” mutant with one basic and one acidic substitution. The roles of the positions of the charged substitutions on dimer formation, the relative oxidative midpoint potentials, and the relative oxidation and reduction rates are discussed.

This dissertation includes my co-authored materials.

## CURRICULUM VITAE

NAME OF AUTHOR: Mark Brimhall Cannon

PLACE OF BIRTH: Salt Lake City, Utah

DATE OF BIRTH: December 20, 1974

## GRADUATE AND UNDERGRADUATE SCHOOLS ATTENDED:

University of Oregon  
Utah State University

## DEGREES AWARDED:

Doctor of Philosophy in Biochemistry, 2005, University of Oregon  
Bachelor of Arts in Chemistry, 2000, Utah State University

## AREAS OF SPECIAL INTEREST:

Protein Engineering  
Redox Biochemistry  
Fluorescence Spectroscopy  
Macromolecular Structure and Function

## PROFESSIONAL EXPERIENCE:

Research Assistant, Institute of Molecular Biology,  
University of Oregon, 2001–2005.

Teaching Assistant, Department of Chemistry,  
University of Oregon, 2000–2001.

Instructor, Computer Science Department,  
Utah State University, 1998–2000.

Teaching Assistant, Department of Chemistry and Biochemistry,  
Utah State University, 2000.

Research Assistant, USDA Forage and Range Research Laboratory,  
Utah State University, 1996–2000.

#### GRANTS, AWARDS AND HONORS:

Dean's List, Utah State University, 1996–1998.

National Institute of Health Training Grant, 2001-2004.

#### PUBLICATIONS:

Hanson, G.T., Aggeler, R., Oglesbee, D., Cannon, M., Capaldi, R.A., Tsien, R.Y., and Remington, S.J. 2004. Investigating mitochondrial redox potential with redox-sensitive green fluorescent protein indicators. *J Biol Chem* **279**: 13044-13053.

Cannon, M. and Remington, S.J. 2005. Re-engineering redox-sensitive green fluorescent protein for improved response rate. [Manuscript in Preparation].



## ACKNOWLEDGMENTS

One does not make it far through the jungles of grad school without the help and support of friends and family, colleagues and coworkers. I would like to acknowledge fellow grad students Dave Anstrom, Dan Yarbrough, George Hanson, Jeremy Lohman, Nathan Henderson, and Xiaokun Shu for explanations, wisdom, critical advice, Taco-Tuesday, and making the Remington Lab a great place to work. Karen Kallio and Leslie Colip are some of the best lab technicians around. Brian Matthews and members of his lab have been an important resource for wisdom and experience in crystallography and science in general. My thesis committee, including Brian Matthews, Bruce Branchaud, Bea Darimont, and Diane Hawley, has been very helpful throughout this process. My advisor, Jim Remington, not only has the most exciting research projects in the institute but is also a passionate, top-notch researcher and I am indebted to him for his patience and support.

Perhaps most importantly, for me, has been the love and encouragement of my family, especially my wonderful wife, Stacey.

## DEDICATION

For Stacey

## TABLE OF CONTENTS

Chapter	Page
I. INTRODUCTION .....	1
Cysteine Chemistry in Biological Systems .....	2
The Green Fluorescent Protein .....	7
GFP as a “Biosensor” .....	16
Research Focus .....	19
II. RE-ENGINEERING ROGFP: BIOCHEMISTRY .....	21
Summary .....	21
Introduction .....	22
Results .....	24
Spectroscopic properties .....	24
Characterization of rate constants .....	27
Ionic strength dependence of rate enhancement .....	30
Characterization of rate constants for oxidation with H <sub>2</sub> O <sub>2</sub> .....	30
Redox midpoint potentials .....	32
Discussion .....	32
Materials and Methods .....	37
Gene construction and protein expression/purification .....	38
Ratiometric fluorescence measurements .....	39
Determination of quantum yield .....	40
Rate determinations .....	40
Midpoint determinations .....	42
III. RE-ENGINEERING ROGFP: STRUCTURAL STUDIES .....	44
Summary .....	44
Results .....	45
Crystal structure analysis of R7 .....	45
Crystal structure analysis of R8 .....	54
Electrostatics calculations .....	57
Discussion .....	63
Rate enhancements .....	63
Midpoint potential .....	64
Materials and Methods .....	66
Crystal structure determinations .....	66
Electrostatics calculations .....	67

Chapter	Page
IV. CONCLUSIONS .....	69
Future Directions .....	70
BIBLIOGRAPHY .....	75

## LIST OF FIGURES

Figure	Page
1. Horf6, a Human Peroxiredoxin .....	6
2. Mechanism for the Formation of the GFP Chromophore .....	9
3. Fluorescence Excitation Spectrum of Wild-Type GFP.....	11
4. Schematic of GFP Excitation and Emission Pathways.....	12
5. Proposed Mechanism for GFP Dual-Excitation .....	14
6. Comparing a Nonratiometric Response with a Ratiometric Response.....	15
7. Excitation Spectra of a RoGFP Variant as it is Reduced.....	26
8. A Comparison of the Reduction Rates for Several of the Variants .....	28
9. First-order Rate Constants Compared at Low and High Salt .....	31
10. Redox Titration of a Representative RoGFP1 Variant .....	33
11. Comparison of $k_{\text{DTT}}$ with Midpoint Potential.....	34
12. DTT Buffer Composition vs. Fraction of Protein Reduced.....	43
13. An Alignment of the A-Molecules of R7 and Wild-Type GFP .....	48
14. The “Active-Site” of R7.....	52
15. Stereo Image of R7.....	53
16. Overlay of R7 and R8 Active-Sites.....	55
17. The “Active-Site” of R8.....	56
18. Calculated vs. Experimentally Observed Rate Enhancements for R7 .....	61
19. Calculated vs. Experimentally Observed Rate Enhancements for R8 .....	62
20. A Stereo Image of an Overlay of the Disulfides of R7 and CD4 D2 .....	74

## LIST OF TABLES

Table	Page
1. Summary of Spectroscopic Properties for RoGFP1-R Mutants .....	25
2. Summary of Kinetic Parameters for RoGFP1-R Mutants .....	29
3. Data Collection and Refinement Statistics for Oxidized R7 and Reduced R8 ..	47
4. Comparison of Dimer Contacts .....	50
5. Comparison of Disulfide Torsion Angles .....	58
6. Calculated vs. Experimental Rate Enhancements .....	60

## CHAPTER I. INTRODUCTION

Among the dangers of life in an aerobic environment is the accumulation of reactive oxygen species (ROS) within cells. Superoxide anions ( $O_2^{\cdot-}$ ) are produced constantly as a byproduct of aerobic metabolism, and are then spontaneously or enzymatically converted to hydrogen peroxide ( $H_2O_2$ ), which can then produce very reactive hydroxyl radicals ( $HO^{\cdot}$ ) through the metal-catalyzed Fenton reaction. ROS are also produced in cells exposed to radiation, inflammatory systems, environmental pollutants, metal ions, etc. Toxic effects of intracellular ROS production include damage to proteins, cell membranes, and nucleic acids. For these reasons all aerobic cells are equipped with machinery to eradicate ROS. These include enzymes such as catalase, glutathione peroxidase, superoxide dismutase, and peroxiredoxins (Rhee 1999) whereas redox buffering systems such as the GSSG/GSH pair also serve as protection against ROS (Chesney et al. 1996). ROS-mediated oxidation of cysteine residues can confer a conformational change to proteins and so is employed by cells to provide a direct response to ROS levels. However, it is becoming increasingly

clear that ROS play other important roles within cells, including acting as second-messenger in cell signaling events. In fact, cysteine thiol oxidation may rival protein phosphorylation for importance in cell signaling.

### Cysteine Chemistry in Biological Systems

Cysteine residues are unique among amino acids in that their side chain contains a reactive thiol group (Cys-SH). The chemistry of this thiol group defines the role that cysteine residues can play in biological systems. Cysteines have an average occurrence in proteins of only 1.9%, the second rarest amino acid behind tryptophan (1.4% occurrence) (Voet et al. 1999) possibly due to the variety of reactions in which they can participate, including oxidation by reactive oxygen species (ROS). Oxidation of the cysteine thiol (Cys-SH), or thiolate (Cys-S<sup>-</sup>) can result in cysteine sulfenic acid (Cys-SOH), sulfinic acid (Cys-SO<sub>2</sub>), or sulfonic acid (Cys-SO<sub>3</sub>), a disulfide bond with another thiol (Cys-S-S-R), an S-nitrosothiol (Cys-S-NO), or even a cyclic sulfenamide (Cys-S-NH-R) (Salmeen et al. 2003; van Montfort et al. 2003) with the cysteine sulfur covalently bound to its main chain nitrogen. All of these oxidized forms can be reversed by reaction with reduced thiols except the double and triple oxidation states of cysteine, sulfinic and sulfonic acids,



respectively, which are considered stable dead-end products. There is, however, some evidence for the enzyme catalyzed reversibility of cysteine sulfinic acid (Biteau et al. 2003).

Because the cysteine thiolate is a much more nucleophilic species than is the thiol form, deprotonation of the thiol is considered to be necessary for these oxidation reactions, including disulfide formation, to occur. These oxidation processes, therefore, are pH-dependent and allow for precise regulation as the reactivity of the cysteine to ROS can be controlled through modulation of the thiol  $pK_a$  by proximity to hydrogen bond donors, basic groups, or metal ions.

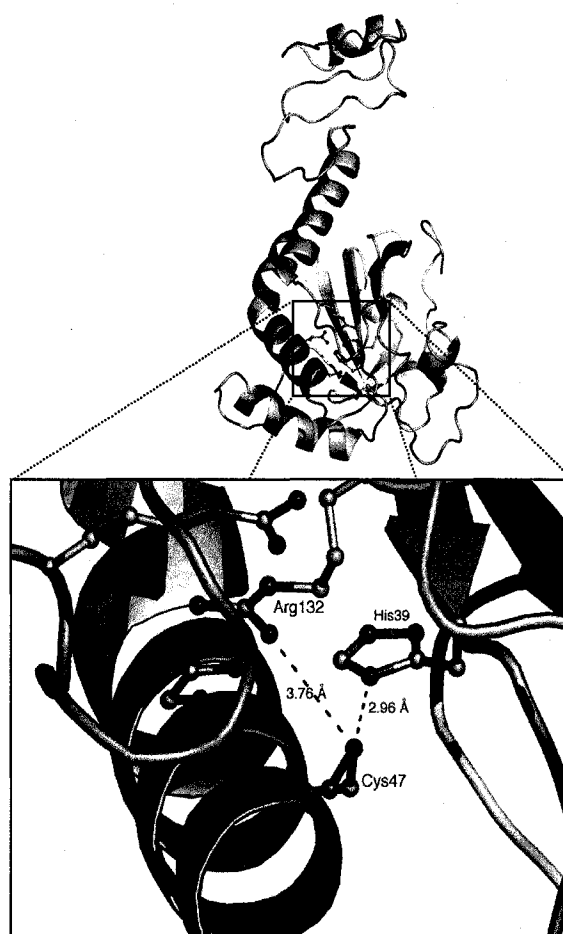
It has long been known that cysteine residues play an important role in protein folding, stabilizing folded states through intramolecular disulfide bond formation. The importance of cysteine reactivity towards ROS in the more dynamic processes of gene regulation, oxidative stress response, and cell signaling has come to light more recently. Substantial evidence implicates ROS, and, in particular,  $H_2O_2$ , as an important second messenger in cell signaling because it is produced in response to various extracellular stimuli, such as cytokines and peptide growth factors, and its intracellular production or exogenous application affects the function of a variety of proteins, including protein kinases, protein phosphatases, ion channels, and transcription factors (Finkel 1998; Rhee et al. 2000; Rhee et al. 2003). However, low levels of  $H_2O_2$  are constantly produced by reactions in aerobic metabolism and therefore all aerobic cells are equipped with defense mechanisms to quickly eliminate

H<sub>2</sub>O<sub>2</sub> (see above). Signaling events like those involving bursts of H<sub>2</sub>O<sub>2</sub> are therefore thought to be quite transient and restricted to microdomains of the cell (Rhee et al. 2000).

Some examples will illustrate the variety of pathways utilized by enzymes to respond to H<sub>2</sub>O<sub>2</sub> and other ROS: The bacterial transcription factor OxyR is involved in the regulation of genes necessary for oxidative stress response. When OxyR Cys199 is oxidized by H<sub>2</sub>O<sub>2</sub> it forms an intramolecular disulfide bond with Cys208, which causes large conformational changes that activate it as a transcription factor (Paget and Buttner 2003). In yeast, the role of transcription factor for oxidative stress is filled by Yap1. A member of the peroxiredoxin superfamily, Orp1, activates Yap1 by disulfide exchange when Orp1 is oxidized by H<sub>2</sub>O<sub>2</sub>. The resultant intramolecular disulfide in Yap1 masks a nuclear export signal, allowing Yap1 to induce gene expression (Delaunay et al. 2002). Peroxiredoxins (Prx) are a family of peroxidases ubiquitous from bacteria to eukaryotes. Oxidation of the peroxidatic cysteine by H<sub>2</sub>O<sub>2</sub> reduces the peroxide and, in some Prx, can further result in intermolecular disulfide bonds that can cause multimeric Prx complexes that act as chaperones (Barford 2004). Protein tyrosine phosphatases employ an active site cysteine that participates in the enzymatic dephosphorylation of protein substrates. Oxidation of this cysteine residue by H<sub>2</sub>O<sub>2</sub> forms cysteine sulfenic acid, which blocks its nucleophilic catalytic activity (Rhee et al. 2000).

These H<sub>2</sub>O<sub>2</sub> sensitive cysteine residues share some common structural attributes. For example, HORF6, a human 1-Cys peroxiredoxin, has an active-site cysteine in a positively charged pocket (see Figure 1) with a neighboring arginine and histidine (Choi et al. 1998). Indeed, all peroxiredoxins have a reactive cysteine with a conserved arginine nearby (Rhee et al. 2001; Hofmann et al. 2002). All protein tyrosine phosphatases have a signature active site motif His-Cys-X-X-Gly-X-X-Arg-Ser/Thr (where X is any amino acid) that places positive charges near the reactive cysteine (Rhee et al. 2000). The presence of conserved basic residues and hydrogen-bond donors near the active-site cysteine serves to stabilize the deprotonated form of the cysteine and thus effectively lower the thiol pK<sub>a</sub>. This is necessary because of the much higher nucleophilicity of the thiolate vs. the cysteine thiol, and because a pK<sub>a</sub> much lower than the textbook value of 8.4 (Voet et al. 1999) is necessary to expect any significant fraction of the cysteine thiol to be deprotonated at biological pH. Although the importance of thiol oxidation-mediated regulation in cellular systems is undeniable, there is still much to learn about how these pathways are initiated, regulated and responded to. Unfortunately, conventional methods for determining cellular thiol redox status require grinding up the cells of interest and quantifying some thiol-bound label, a decidedly invasive procedure with little or no spatial or temporal resolution. However, green fluorescent protein (GFP) based biosensors have been developed that respond to *in vivo* thiol oxidation levels with ratiometric fluorescence changes (Hanson et al. 2004). These probes are genetically encoded and

Figure 1. Horf6, a human peroxiredoxin. The active-site peroxidatic cysteine, Cys47 (here shown as a sulfenic acid), is near basic residues and hydrogen-bond donors, which activate the thiol. (Figure made using the Protein Data Bank file 1PRX and PyMOL molecular viewing software (DeLano 2002).)



therefore can be targeted to specific subcellular locations and monitored in “real time”. In subsequent sections of this chapter, background will be given about GFP and its use as a fluorescent biosensor, including as a reporter of thiol redox events.

### The Green Fluorescent Protein

*Aequorea victoria*, or “crystal jelly”, is a colorless jellyfish with an adult size of 5–10 cm that is abundant in the Pacific Ocean near the northwest coast of the United States. These animals bioluminesce when physically agitated, with luminescence appearing as small green beads of illumination around the rim of the bell (Mills 2004). Luminescence is produced by the protein aequorin which binds  $\text{Ca}^{2+}$  and emits blue photons as one of the products in a decomposition reaction (Shimomura and Johnson 1973). This blue light is absorbed by green fluorescent protein (GFP) and emitted as green fluorescence. It is unknown why these creatures expend valuable cellular energy to produce light and why extra protein machinery is used to convert the blue light to green. However, in the past 13 years since it was cloned from *Aequorea*, this accessory protein has become one of the most widely used molecular labeling tools in biology (Prasher et al. 1992).

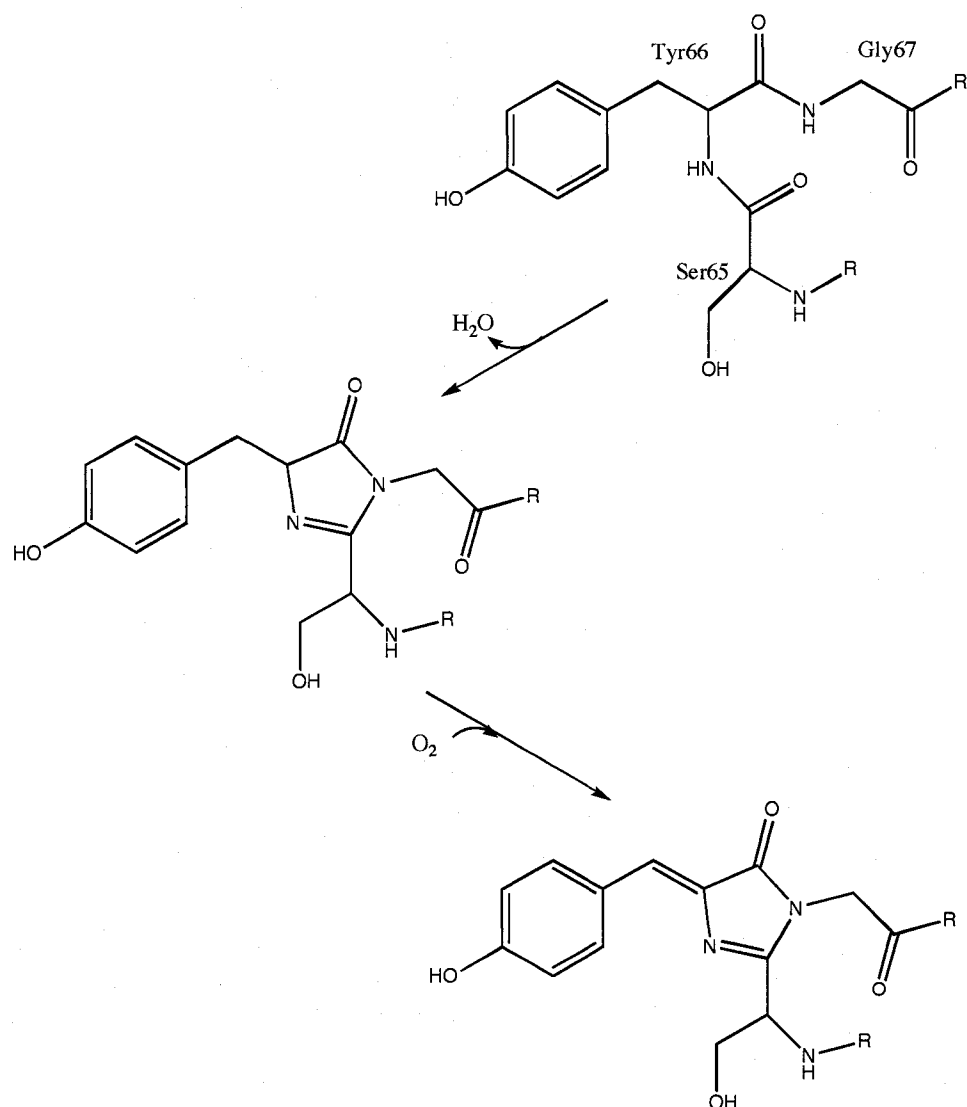
The *Aequorea victoria* green fluorescent protein is a small protein of 238 amino acids and molecular weight of about 26 kD. Its structure is a nearly perfect

barrel shape composed of 11 antiparallel  $\beta$ -strands surrounding a rather distorted coaxial  $\alpha$ -helix (Ormo et al. 1996; Yang et al. 1996). This “ $\beta$ -barrel” is capped on both ends by short helices and loops that allow almost no solvent accessibility to the interior of the structure. Three sequential residues on the interior coaxial helix, Ser65, Tyr66 and Gly67, spontaneously form the green light-emitting 4-(*p*-hydroxybenzylidene)imidazolidin-5-one chromophore (see Figure 2). Nucleophilic attack of the amide nitrogen of Gly67 on the carbonyl carbon of Ser65 forms a five-membered imidazolone ring. This is followed by dehydration of the carbonyl oxygen of Ser65 and the much slower step of oxidation of the Tyr66 C $\alpha$ –C $\beta$  bond to complete the conjugation of the ring systems (Heim et al. 1994). This process requires no accessory proteins or external cofactors other than molecular oxygen.

GFP is extremely protease resistant, and remains stable under very denaturing conditions. It is genetically encoded and produces bright green fluorescence without any cofactors or accessory proteins, while tolerating both N- and C-terminal fusions. For these reasons it has been widely used as a fusion-tag in many systems, both prokaryotic and eukaryotic (Tsien 1998).

Although several GFP homologues have been isolated from marine organisms, with a rainbow of emission colors ranging from cyan to yellow to red (Matz et al. 1999; Labas et al. 2002), GFP is still unique in its complex excitation/emission spectra. Wild-type GFP has two excitation peaks: a major peak at about 395 nm, and a minor peak at about 475 nm with about one-third the amplitude of the major peak

Figure 2. Mechanism for the formation of the GFP chromophore from three internal residues: a cyclization reaction followed by oxidation of the Tyr65 side chain to complete the conjugation of the chromophore ring system.



(see Figure 3). Excitation at either peak causes green emission at 508 nm. The presence of two separate excitation peaks suggests that two distinct chromophore states exist with similar emission wavelengths.

Prior to the crystal structure of GFP being published, Chattoraj and coworkers, using time-resolved fluorescence, untangled the GFP excited state kinetics to explain the unique dual-excitation properties of the GFP chromophore. They showed that excitation at the lower-energy band (at about 475 nm) leads to essentially instantaneous fluorescence emission at 508 nm, whereas excitation at the higher-energy wavelength (at about 395 nm) leads to immediate blue fluorescence emission at 460 nm which rapidly decays with a concomitant increase in green fluorescence (508 nm) over a timescale of only a few ps (Chattoraj et al. 1996). Because deuterated GFP excited with 398-nm light responded in the same manner but with significantly slower kinetics, the authors concluded that a proton transfer reaction transforms the blue emitting species into a green emitting intermediate species, corresponding to different protonated/excited states of the chromophore (see Figure 4). By comparing the crystal structure of S65T GFP (Ormo et al. 1996) to that of wild-type GFP, Brejc *et al.* were able to propose a structural basis for dual excitation that agreed well with the scheme put forth by Chattoraj and coworkers (Brejc et al. 1997). The structures are essentially identical except for some key differences in residues near the chromophore that act to either stabilize the anionic phenolate form



Figure 3. Fluorescence excitation spectrum of wild-type GFP with emission measured at 510 nm. The major peak at 395 nm (A band) corresponds to the neutral form of the chromophore, whereas the minor peak at 475 nm (B band) corresponds to the anionic chromophore.

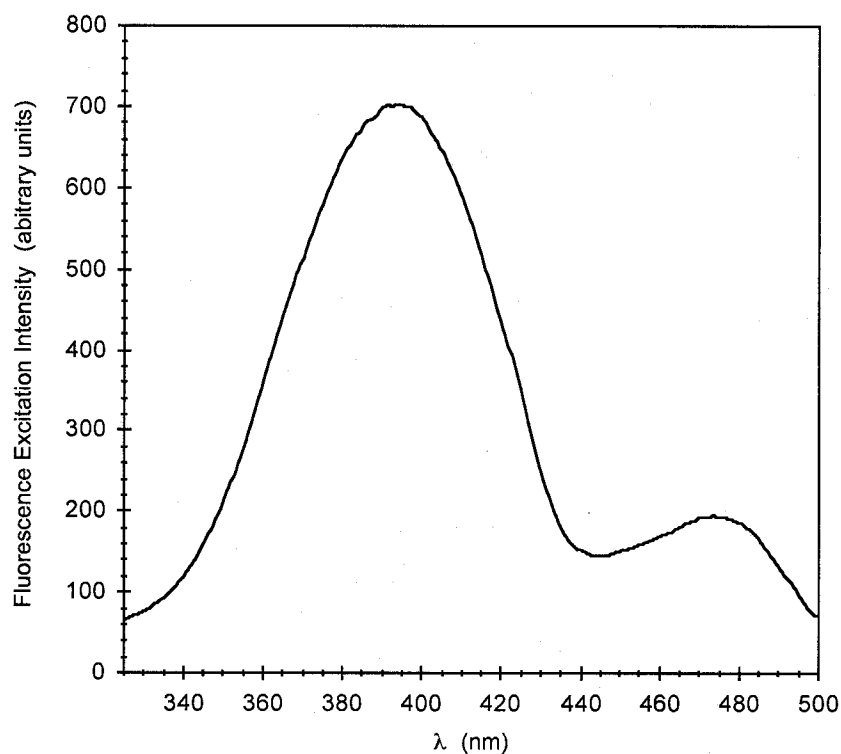
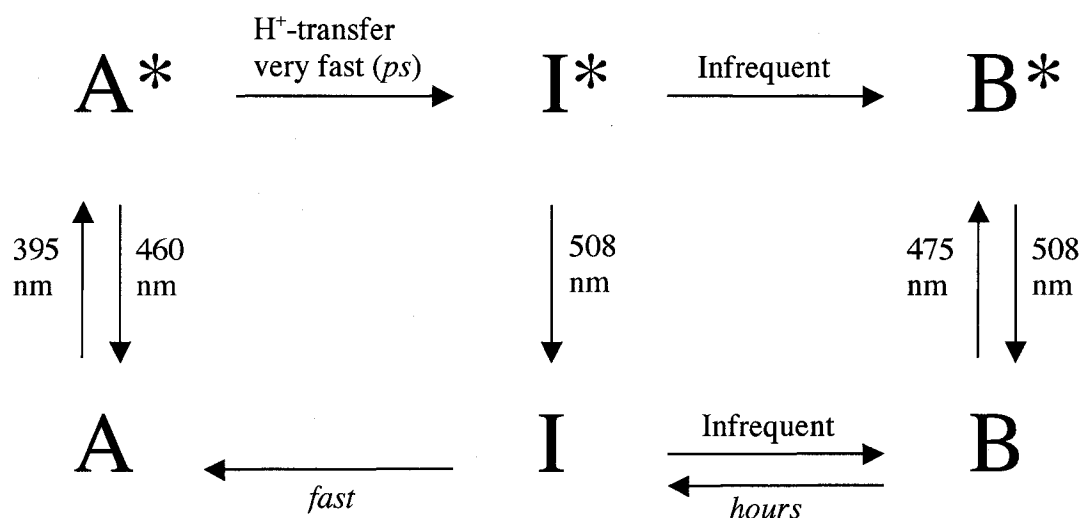


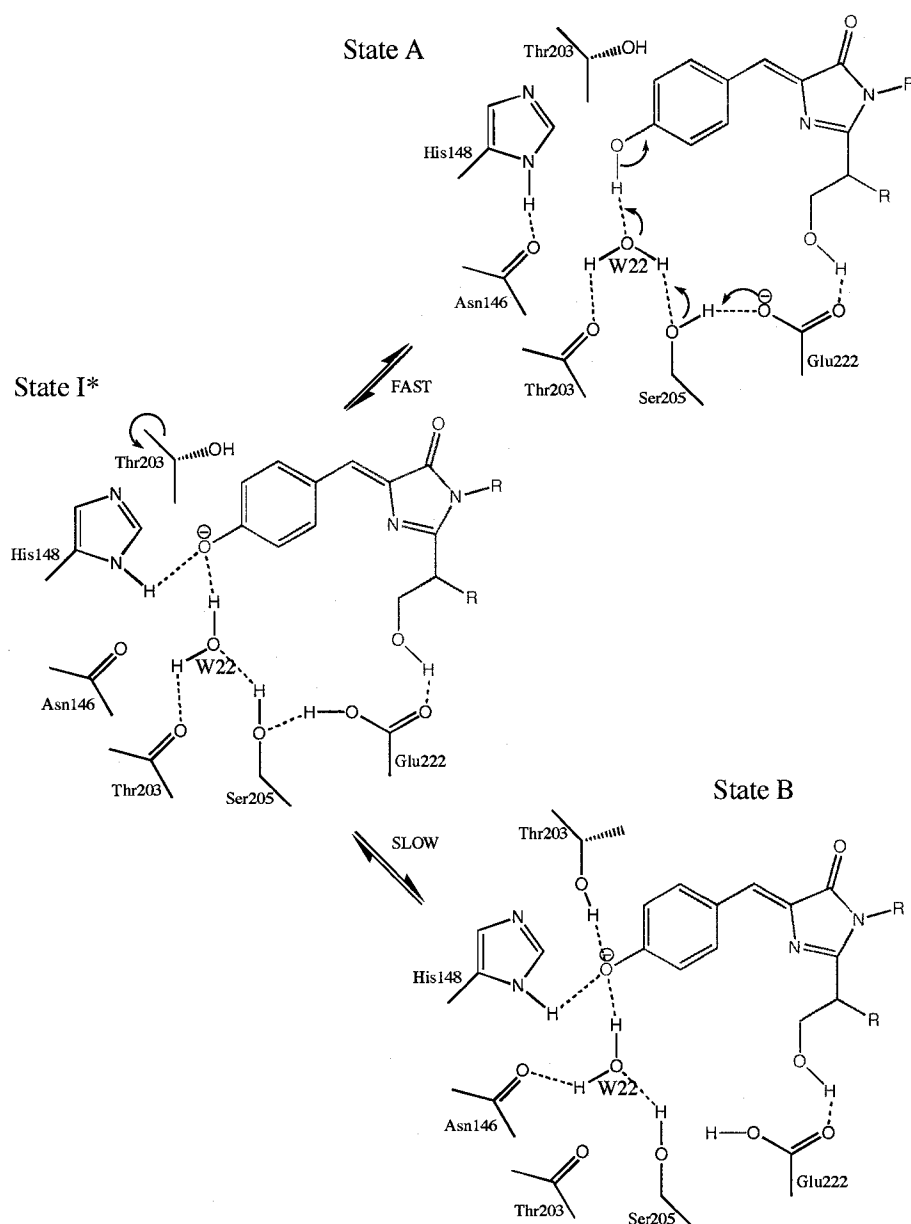
Figure 4. Schematic of GFP excitation and emission pathways. “A” is the neutral and “B” the anionic form of the chromophore. Excitation of the A-state causes a proton transfer reaction that forms the anionic intermediate “I\*” state. I\* quickly emits a green photon and relaxes back to the A-state. Modified from (Chattoraj et al. 1996).



of the chromophore (as in S65T) or the neutral phenolic chromophore (wild-type). Using this structural information the authors were able to propose a mechanism for the photoisomerization of the chromophore (see Figure 5): In wild-type GFP the chromophore is maintained in the neutral form (state A) by hydrogen bonding networks that include the charged side chain of Glu222 stabilizing the phenolic hydroxyl with a hydrogen bond through the carbonyl oxygen of Asn146 and a water molecule (W22). As the chromophore absorbs light energy it moves to an excited state (state A\*) which rapidly isomerizes to an anionic excited state (state I\*) through donation of the charge on Glu222 to the Tyr66 side chain by excited state proton transfer through the hydrogen-bonding network of Glu222–Asn146–W22–Tyr66. The negative charge is then stabilized by new interactions, including the side chain of His148 donating a hydrogen-bond to the phenolate of Tyr66 (Brejc et al. 1997). A comparison of the crystal structures of the GFP S65T mutant by Elsliger *et al.* at low and high pH bolsters this mechanism as the only structural differences between these two structures at pH above and below the expected  $pK_a$  of the chromophore are that those consistent with titration of the phenolic hydroxyl group (Elslinger et al. 1999). Although merely a complication to those only interested in GFP as a passive tag, the dual-excitation behavior of wild-type GFP allows the construction of GFP based “ratiometric” biosensors.

A reporter that responds to an environmental stimulus with only an increase or decrease in overall fluorescence is subject to a considerable amount of potential

Figure 5. Proposed mechanism for GFP dual-excitation. Excited-state proton transfer converts the blue-emitting state A into a green-emitting state I\* on a very fast timescale.



measurement error because fluorescence intensity is also dependent on many other poorly understood or variable factors (illumination intensity, variable cell wall thickness, and variable indicator concentration, to name a few). A ratiometric reporter displays two excitation or two emission intensities with an opposite response to an environmental stimulus (Figure 6 compares a ratiometric to a non-ratiometric response). This allows the quantification of the stimulus through measurement of a ratio of fluorescence intensities. Because this ratio is independent of *overall* fluorescence intensity, it is not affected by the problems stemming from the variable factors described above (Grynkiewicz et al. 1985).

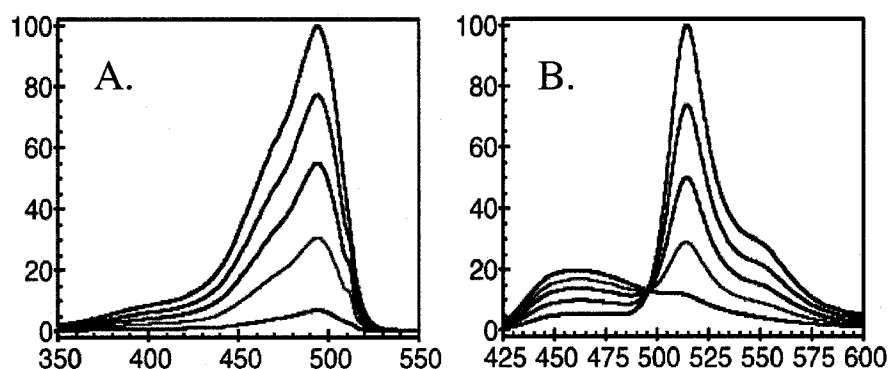


Figure 6. Comparing: (A) a nonratiometric response with, (B) a ratiometric response.

### GFP as a “Biosensor”

Since the cloning of *Aequorea* GFP, its most common usage has been as a passive indicator for spatial and temporal protein localization (Zhang et al. 2002). Because GFP is genetically encoded and requires no external factors for chromophore maturation (except O<sub>2</sub>), it is quite easily fused to proteins of interest by genetic manipulation and visualized by fluorescence microscopy. However, more recently it has been the basis of active fluorescent sensors of various cellular phenomena.

Several novel applications of fluorescent proteins have been developed on the basis of fluorescence (or Förster) resonance energy transfer (FRET) between GFP mutants. Fluorescent molecules with overlapping excitation and emission spectra can participate in FRET, where the donor fluorophore emission can excite the acceptor fluorophore when the two are within close (roughly < 50 Å apart) molecular proximity to each other (Jares-Erijman and Jovin 2003). This can be monitored by measuring the ratio of emission of the two fluorophores, because donor fluorophore emission is converted into acceptor fluorophore emission when FRET occurs. FRET-based biosensors have been developed based on GFP mutants to report on Ca<sup>2+</sup> concentrations, protease activities, kinase activities, and protein–protein interactions (Zhang et al. 2002; Griesbeck 2004). This is usually accomplished by the fusion of a

donor GFP mutant (e.g. blue fluorescent protein, BFP, a variant of GFP (Heim et al. 1994)) to one terminus of a sensor protein and an acceptor GFP mutant (e.g. yellow fluorescent protein, YFP, another GFP variant (Ormo et al. 1996)) to the other terminus of the sensor protein. Conformational changes in the sensor protein (e.g. calmodulin) upon ligand binding or side chain modification change the proximity of the donor–acceptor pair and thus the FRET efficiency. This technique is limited by the availability of specific sensor proteins that make large conformation changes in the presence of the property of interest. Intermolecular FRET-based indicators suffer from problems of calibration as the ratio of donor and acceptor is not fixed. False negatives due to unexpected interactions involving one of the donor–acceptor fluorophores, and nonideal interaction geometries also lead to complications.

Fluorescent biosensors have been successfully developed based on the modification, by site-directed or random mutagenesis, of the fluorescent properties of GFP variants to respond to environmental stimuli. These eliminate many of the problems of the FRET-based applications discussed above (although they are not without their own problems). GFP is inherently pH-sensitive; that is, overall fluorescence deteriorates as pH drops below the  $pK_a$  of the chromophore (Wachter et al. 1997). This attribute has been exploited, using wild-type GFP or  $pK_a$ -modifying mutants, to measure intracellular pH's (Kneen et al. 1998; Llopis et al. 1998). Next generation pH-sensors include GFP mutants ratiometric by excitation, termed “pHluorins” (Miesenbock et al. 1998), and “deGFPs” that are ratiometric by opposing

changes in blue and green emission (Hanson et al. 2002). The yellow variant of GFP, YFP, has been shown to be sensitive not only to pH but also to halides (Wachter and Remington 1999; Wachter et al. 2000), and has been used to probe intracellular chloride levels (Jayaraman et al. 2000). The blue variant of GFP, BFP, has been further modified to serve as a Zn(I) and Zn(II) sensor, essentially by mutating a surface residue to allow solvent access to the histidine-containing BFP chromophore which resembles a Zn binding site (Barondeau et al. 2002).

The application of GFP as a biosensor with which this dissertation is concerned is that of probing thiol redox status. Redox-sensitive versions of GFP have been developed. These probes, termed “roGFPs”, which respond reversibly to redox levels with a ratiometric change in fluorescence excitation, were developed by placing pairs of cysteine residues on neighboring strands of the surface of the GFP  $\beta$ -barrel in positions that allow disulfide formation (Hanson et al. 2004). A crystal structure of roGFP2 shows that disulfide formation between the pair of engineered surface cysteine residues results in a shift of one  $\beta$ -strand relative to the other (Hanson et al. 2004). This causes subtle internal structural rearrangements, including re-positioning of side chains contacting the chromophore that favor the neutral chromophore over the anionic (i.e. His148, Ser205), so that as a population of roGFP is oxidized the excitation peak at 475 nm is decreased while the 395-nm peak is increased. RoGFPs were expressed in mammalian cells and were shown to be effective indicators of one



or more of the contributing factors to the ambient cellular redox potential, as perturbed by exogenous oxidants and reductants, as well as by physiological redox changes (Dooley et al. 2004; Rossignol et al. 2004).

Redox-sensitive versions of YFP have also been developed, termed “rxYFP”, which reversibly respond to disulfide formation, but with a nonratiometric, overall decrease in fluorescence intensity (Ostergaard et al. 2001).

### Research Focus

RoGFPs are valuable tools for the study of redox processes within the cell because they are genetically encoded and can be targeted to specific subcellular locations where their response to redox changes can be monitored in real-time with a minimum of invasiveness to the system of interest. However, roGFPs suffer from two serious problems that limit their usefulness in some interesting cellular systems. First, the response time of the roGFP probes, measured in some tens of minutes (Dooley et al. 2004), is too slow for use in many interesting applications. The study of dynamic redox systems, where oxidants or reductants are generated in microdomains of the cell (e.g.  $\text{H}_2\text{O}_2$  generation as a second messenger in cell signaling (Rhee et al. 2000)) and then are quickly degraded due to their potential for long-term toxicity, might be impossible with the present roGFPs because these quick

reaction cycles would likely not allow the probes sufficient time to produce a measurable response. Secondly, roGFPs were reported to have very similar and very reducing midpoint potentials (Hanson et al. 2004). RoGFPs targeted to subcellular organelles with significantly more oxidizing ambient redox levels would be completely oxidized and therefore unable to report subtle changes in the redox environment.

The focus of my research has been to re-engineer roGFPs to minimize the problem of slow roGFP response times, and, to a lesser extent, to develop roGFPs with a broader range of disulfide midpoint potentials. This has been done by re-engineering the roGFP protein surface to more closely resemble naturally occurring enzymes with very reactive active-site cysteines.

## CHAPTER II. RE-ENGINEERING roGFP: BIOCHEMISTRY

### Summary

In this chapter I describe the modification of roGFP1 (GFP with C48S/S147C/Q204C) (Hanson et al. 2004), in order to address the roGFP problems of slow response and reducing midpoint, producing several mutants with increased basicity around the surface cysteine residues. Biochemical evidence is given showing significantly faster rates of response, in vitro, to DTT and  $\text{H}_2\text{O}_2$  for most of these mutants, with increasing numbers of added basic groups corresponding to increasing rate. Midpoint becomes slightly more oxidizing with increasing basicity, and the ionic strength-dependency of the rates also supports the idea that electrostatic contributions from the nearby basic substitutions decrease the cysteine  $\text{pK}_a$ 's.

## Introduction

The *Aequorea* green fluorescent protein has two widely separated excitation maxima whose ratio depends on the structure of the molecule and can hence depend on external conditions (Ormo et al. 1996; Tsien 1998). This feature, which is unique among fluorescent proteins characterized to date allows the construction of ratiometric indicators which can be targeted to subcellular organelles (Nagai et al. 2001; Hanson et al. 2002). Redox-sensitive probes have been developed based on this principle (designated roGFP1–6, see Chapter 1). However, preliminary data suggest that two problems will limit the usefulness of these probes in some applications: (1) the slow response rate of roGFPs to stepwise changes in redox potential, some tens of minutes, and; (2) very reducing midpoint potentials, as indicated by titration against small molecule thiols.

By modifying the environment of the engineered cysteine residues in roGFP to resemble naturally occurring redox-sensitive enzymes, specifically by adding basic residues to decrease the cysteine thiol  $pK_a$ , it is possible to increase the reaction rate of the disulfide chemistry. There are many examples in the literature of significant changes in cysteine reactivity resulting from the modification of charged residues near an active-site cysteine residue. Zhang et al. showed that the substitution of His402, a conserved basic residue next to the active-site Cys403 of *Yersinia* protein tyrosine phosphatase, with asparagine and alanine resulted in a thiol  $pK_a$  shifts of 4.67

to 5.99 and 7.35, respectively (Zhang and Dixon 1993). Dyson and coworkers did a study of thiol reactivity in *E. coli* thioredoxin in which they showed that mutation of Asp26 and Lys57, two conserved, buried residues near the active-site cysteines, to alanine and methionine had a significant effect on the cysteine  $pK_a$  as well as on the enzyme's redox reaction rates (a 40-fold decrease in  $k_{cat}/K_m$  for the double mutant) (Dyson et al. 1997). Ferredoxin:thioredoxin reductase (FTR) is a key redox regulatory enzyme in oxygenic photosynthetic cells that uses a 4Fe–4S cluster and an adjacent active-site disulfide to catalyze the two-electron reduction of thioredoxins with electrons from ferredoxin. Glauser et al. replaced His86, next to the active-site disulfide of FTR, with a tyrosine and demonstrated a 90% decrease in activity for the mutant relative to wild-type protein (Glauser et al. 2004). Dooley et al. reported that the substitution of positive charges near the disulfide of roGFP2 increased reactivity towards  $H_2O_2$  in vitro as well as in vivo (Dooley et al. 2004) but did not quantitate this effect. The active sites of many other redox-active enzymes, including the methionine sulfoxide reductase, pilB, have an additional acidic group adjacent to the conserved basic residue, forming a Cys-Arg-Asp/Glu catalytic triad (Lowther et al. 2002).

The primary focus of this work is to improve the response time of roGFPs. However, the second roGFP problem, that of very reducing midpoint potentials, is also partly addressed by the addition of basic residues near the disulfide. This is

because the midpoint potential of the disulfide is at least partly dependent on cysteine  $pK_a$ . Consequently,  $E^{\circ'}$  should become more positive as the cysteine  $pK_a$  decreases (Chivers et al. 1997; Schafer and Buettner 2001).

## Results

### **Spectroscopic properties**

Nine variants of roGFP1 were constructed in which one to four surface residues near the engineered disulfide were replaced with a lysine, an arginine or an aspartate residue (see Table 1). In all cases, titration against a 1 mM DTT redox buffer resulted in fluorescence excitation changes similar to what is seen for the parent roGFP1 (Hanson et al. 2004). Excitation peaks at 395 and 475 nm correspond to the protonated (neutral) and deprotonated (anionic) states of the chromophore, respectively, with most of the intensity at 395 nm (see Figure 7). As the protein is reduced the intensity of the 395-nm peak decreases, whereas that of the 475-nm peak increases. The dynamic range ( $\delta$ , defined as the maximum observed ratio of excitation peak ratios) varies somewhat between mutants from  $\delta_{R11} = 5.4$  to  $\delta_{R8} = 7.5$  compared with  $\delta_{roGFP1} = 6.5$ . The fluorescence quantum yield ( $\Phi$ ) for emission with excitation at 400 nm varies from  $\Phi_{R8} = 0.42$  to  $\Phi_{R10} = 0.65$  with  $\Phi_{roGFP1} = 0.64$ .

Table 1.

*Summary of spectroscopic properties for roGFP1-R mutants*

Variant <sup>a</sup>	ID	$\delta^b$	$\Phi^c$	$\epsilon^d$ M <sup>-1</sup> cm <sup>-1</sup>
S147C/Q204C	roGFP1	6.5	0.64	20200
S147C/Q204C/F223R	R1	5.6	0.60	24100
S147C/Q204C/N149K	R3	7.0	0.58	20100
S147C/Q204C/F223R/S202K	R7	6.2	0.64	25700
S147C/Q204C/F223R/K41D	R8	7.5	0.42	12600
S147C/Q204C/N149K/Y151D	R9	7.2	0.64	15200
S147C/Q204C/F223R/S202K/K41D	R10	6.2	0.65	22500
S147C/Q204C/N149K/F223R	R11	5.4	0.60	18700
S147C/Q204C/N149K/F223R/S202K	R12	5.6	0.62	23100
S147C/Q204C/N149K/F223R/S202K/Y151D	R14	5.6	0.60	20700

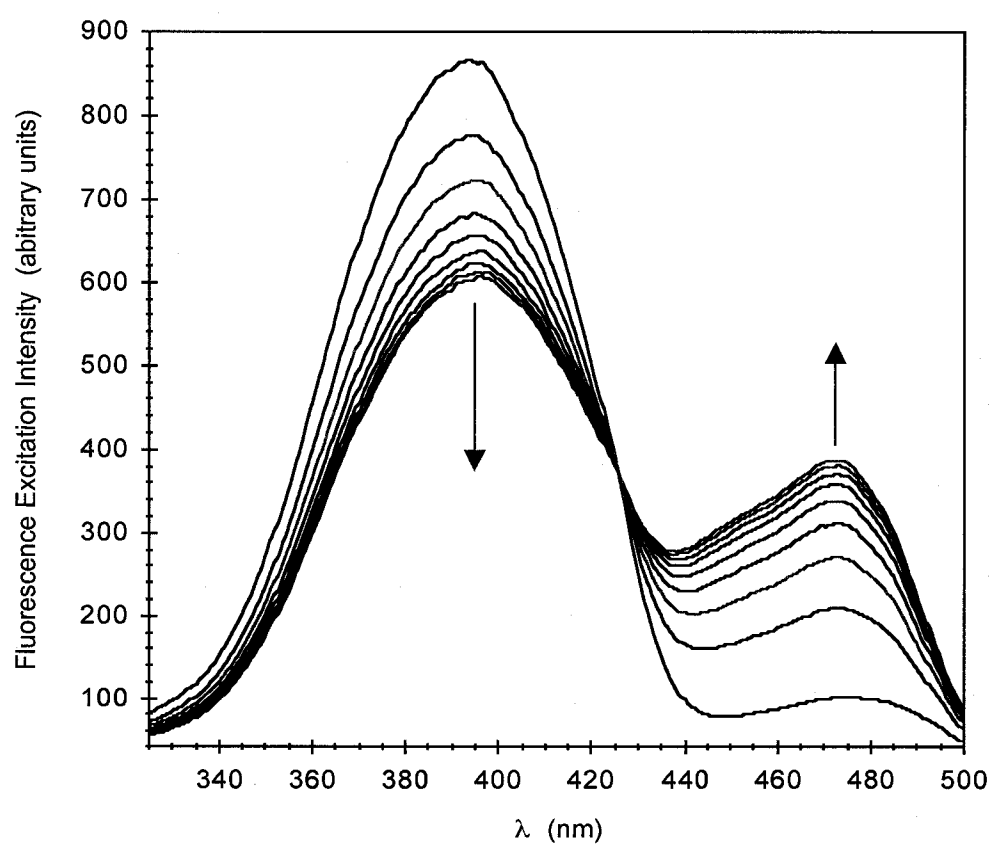
<sup>a</sup> Variants also contain the two phenotypically neutral substitutions C48S and Q80R.

<sup>b</sup> The dynamic range value ( $\delta$ ) is the maximum observed  $\delta$ -fold change in excitation peak ratio.

<sup>c</sup> The fluorescence quantum yield for emission with excitation at 400 nm.

<sup>d</sup> Extinction coefficients for absorbance at 400 nm.

Figure 7. Excitation spectra of a roGFP variant (R9) as it is reduced, with emission measured at 510 nm. Arrows show the direction of change at each peak. Spectra were measured every three minutes after the addition of DTT.





Extinction coefficients ( $\epsilon$ ) for absorbance at 400 nm vary from  $\epsilon_{R8} = 12600 \text{ M}^{-1}\text{cm}^{-1}$  to  $\epsilon_{R7} = 25700 \text{ M}^{-1}\text{cm}^{-1}$  compared with  $\epsilon_{\text{roGFP1}} = 20200 \text{ M}^{-1}\text{cm}^{-1}$ . See Table 1 for complete spectroscopic results.

### Characterization of rate constants

The pseudo-first-order rate constant ( $k$ ) for reduction of each of the variants was determined in low-salt buffer (50 mM HEPES). This was done by monitoring the fluorescence excitation over time, after the addition of a large excess (1 mM) of DTT at pH 7. Rate constants for this disulfide reduction reaction ranged from  $k_{\text{DTT},R8} = 0.09 \text{ min}^{-1}$  to  $k_{\text{DTT},R12} = 0.66 \text{ min}^{-1}$  with  $k_{\text{DTT},\text{roGFP1}} = 0.11 \text{ min}^{-1}$  (see Figure 8).

Table 2 compares these rates. In general, mutants with one basic substitution near the disulfide have approximately double the rate constant of the parent roGFP1, with each additional basic substitution increasing this rate enhancement approximately 2-fold. Introducing an acidic group (aspartate) had different effects depending on context. Rate constants for variants with the acidic substitution K41D were significantly decreased (i.e. compare R8 with R1, R10 with R7) while rate constants for variants with or without the other acidic substitution, Y151D, were essentially unchanged (i.e. R9 and R3, R12 and R14).

Figure 8. A comparison of the reduction rates for several of the variants. Shown is the fraction of protein reduced after addition of 1 mM DTT over time. Pseudo-first-order rate constants were determined by fitting rate curves to a first-order rate equation.

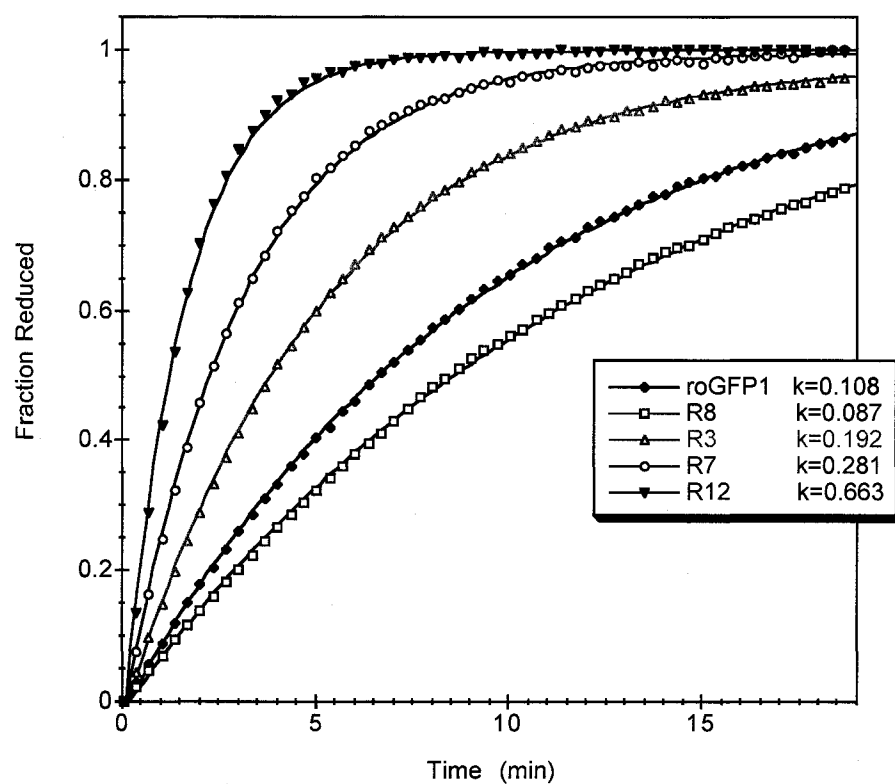


Table 2.

*Summary of kinetic parameters for roGFP1-R mutants*

Variant	$k^a$ (DTT, high salt)	$k^b$ (DTT, low salt)	$k^c$ (H <sub>2</sub> O <sub>2</sub> , low salt)	Eo' (DTT) <sup>d</sup>	Eo' (lipoic acid) <sup>e</sup>
	min <sup>-1</sup>	min <sup>-1</sup>	min <sup>-1</sup>	V	V
R8	0.10	0.09	0.24	-0.284	
roGFP1	0.13	0.11	0.42	-0.281	-0.285
R10	0.12	0.11	0.67	-0.284	
R1	0.16	0.19	0.89	-0.269	
R9	0.17	0.18	0.59	-0.278	
R3	0.15	0.19	0.75	-0.282	
R7	0.19	0.28	1.41	-0.268	
R11	0.22	0.32	0.55	-0.275	
R14	0.31	0.56	1.22	-0.263	
R12	0.29	0.66	2.05	-0.265	

<sup>a</sup> Rate constants (k) here are from the equation  $R = A(1 - e^{-kt}) + B$ , determined at high ionic strength (300 mM NaCl, 50 mM HEPES), using 1 mM DTT.

<sup>b</sup> Rate constants (k) here are from the equation  $R = A(1 - e^{-kt}) + B$ , determined at low ionic strength (0 mM NaCl, 50 mM HEPES), using 1mM DTT.

<sup>c</sup> Rate constants (k) here are from the equation  $R = A(1 - e^{-kt}) + B$ , determined at low ionic strength (0 mM NaCl, 50 mM HEPES), using 1mM H<sub>2</sub>O<sub>2</sub>.

<sup>d</sup> Midpoint potentials from titration against DTT (assumed midpoint potential -323 mV) at 25° and pH 7.

<sup>e</sup> Midpoint potentials from titration against lipoic acid (assumed midpoint potential -290 mV) at 25° and pH 7.

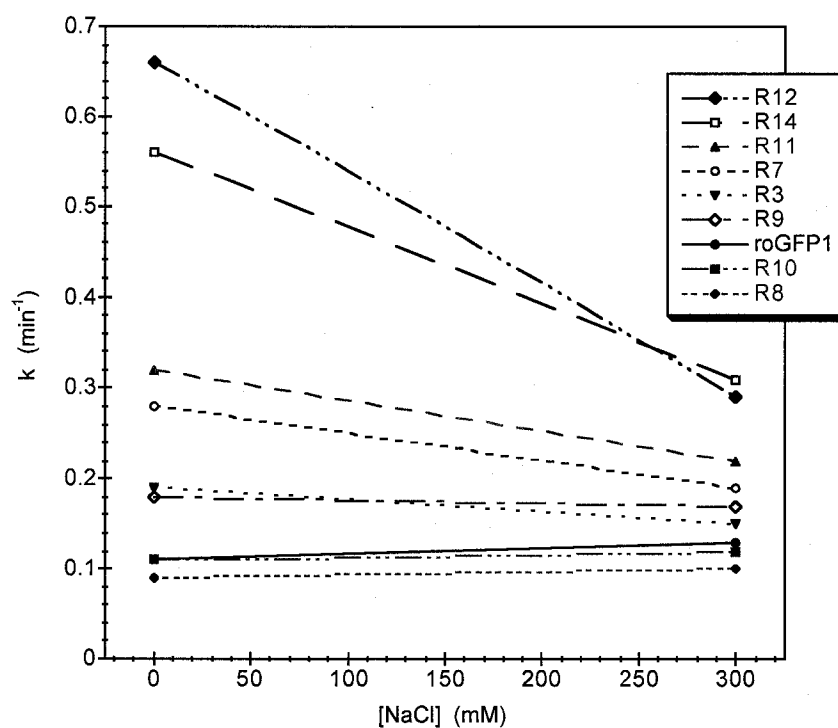
### **Ionic strength dependence of rate enhancement**

To explore the ionic strength dependency of the mutant's redox chemistry the DTT rate constants were measured at pH 7 using NaCl concentrations from 0–300 mM. Results are summarized in Table 2. As expected from Debye screening (Tanford and Kirkwood 1957; Ramos and Baldwin 2002), most of the variants had decreasing rates with increasing salt concentrations, with a greater difference between low and high salt concentration rates observed for mutants with more basic substitutions (see Figure 9). Interestingly, the rate constants for both the parent roGFP1 and variants containing K41D increased with increasing salt concentrations.

### **Characterization of rate constants for oxidation with H<sub>2</sub>O<sub>2</sub>**

To investigate the effect of the charged substitutions on the oxidation reaction, pseudo-first-order rate constants were determined in vitro for each of the mutants using H<sub>2</sub>O<sub>2</sub>. Table 2 compares these rate constants to those measured using DTT. In general, increasing basic charge near the disulfide leads to increasing rates of disulfide formation, similar to what was seen for the disulfide reduction reaction. A comparison of the rate enhancements (compared to the roGFP1 rate constant) for the DTT and the H<sub>2</sub>O<sub>2</sub> reactions gives a correlation coefficient of 0.84. The mutant with the largest difference in rate enhancements was R11, which has  $k_{\text{DTT},\text{R11}}$  that is three times greater than that of roGFP1, while  $k_{\text{H}_2\text{O}_2,\text{R11}}$  is only 1.3 times that of roGFP1 (error for each measurement is less than  $\pm 0.03 \text{ min}^{-1}$ ).

Figure 9. First-order rate constants compared at low and high salt. Mutants with more basic residues show a steeper (*i.e.*, more negative) slope.



### Redox midpoint potentials

The redox midpoint potentials of all the roGFP1 mutants were determined from the equilibrium constant for the reaction of roGFP1 with DTT (see Figure 10), and ranged from  $E^{\circ'}_{R14} = -263$  mV to  $E^{\circ'}_{R8} = -284$  mV (see Table 2). Although the variation is not large between mutants there is a strong correlation between midpoint and the number of basic substitutions, with more positive charges near the disulfide corresponding to more oxidizing midpoint potentials. Figure 11 shows the correlation between  $k_{\text{DTT}}$  and  $E^{\circ'}$ . The correlation coefficient for the comparison of  $k_{\text{DTT}}$  and  $E^{\circ'}$  is 0.84, for  $k_{\text{H}_2\text{O}_2}$  and  $E^{\circ'}$  it is 0.82.

### Discussion

Variants of the redox-sensitive GFP, roGFP1, have been successfully developed with improved response times by modeling the reactive disulfide environment based on those found in naturally occurring redox-sensitive enzymes. The substitution of residues near the disulfide with lysine or arginine caused a significant increase in the rate of disulfide reduction by DTT and the rate of oxidation by  $\text{H}_2\text{O}_2$ . Mutants with up to three new basic residues were developed and each additional positive charge near the disulfide was shown to further increase the rate, up

Figure 10. Redox titration of a representative roGFP1 variant (R3). Midpoints were determined from the  $K_{eq}$  of the reaction of roGFP with DTT. The fraction of protein reduced is determined from the fluorescence spectrum at various ratios of  $DTT_{ox}/DTT_{red}$  (see Materials and Methods for details).

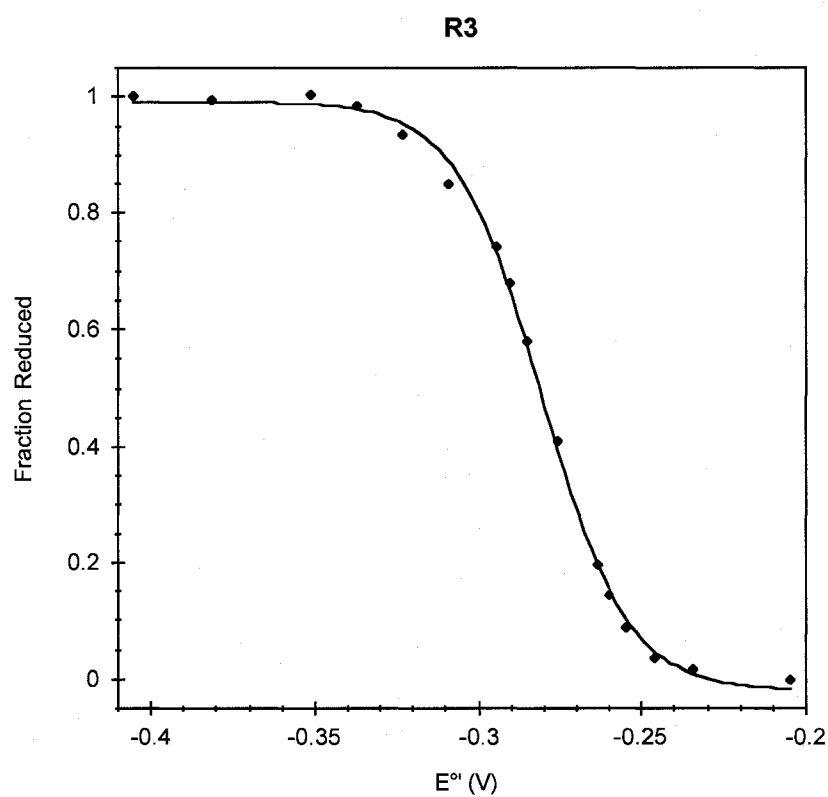
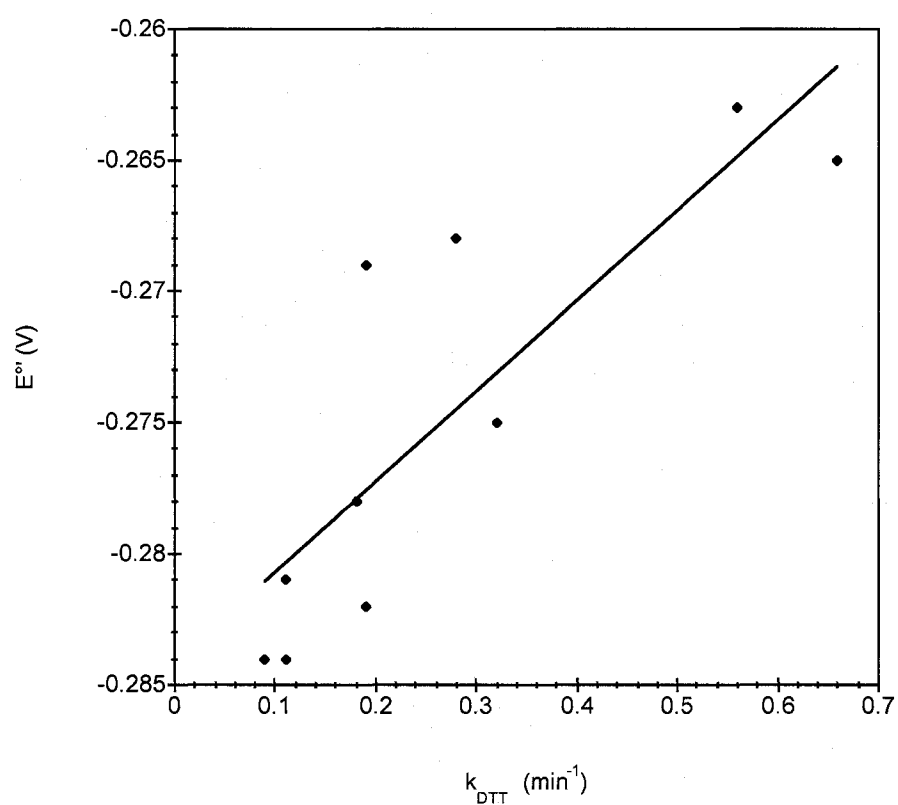


Figure 11. Comparison of  $k_{\text{DTT}}$  with midpoint potential for the mutants. Correlation coefficient for this comparison is 0.84.





to a six-fold increase in the first-order rate constant. These roGFP1 variants will allow the study of many important cellular regulatory events with improved temporal resolution.

The effect of ionic strength on the observed rate enhancement was explored. Increasing salt concentrations led to attenuated rate enhancements for most of the mutants. This is expected, since increasing salt concentrations would provide increased screening of the basic electrostatic contributions to the cysteine  $pK_a$ s. RoGFP1, R8 and R10 were the only variants in which increasing salt concentrations led to increasing rates. This behavior is not surprising since R8 and R10 both have the K41D substitution and this acidic substitution should have the opposite electrostatic effect from that of a basic substitution on a nearby cysteine  $pK_a$ . RoGFP1 has an overall negative charge (theoretical  $pI = 5.8$ , overall charge at neutral pH of about  $-9$ ) and therefore Debye screening by high ionic strength in solution should reduce the effect of these negative charges on the cysteine  $pK_a$ 's. Two mutants, R9 and R14, had a different acidic substitution, Y151D. The effect of this added acidic group on the cysteine  $pK_a$ s appears to be much less significant than the effect of the K41D substitution because the behavior of these mutants over the range of ionic strengths tested is similar to that of the variants with the same basic substitutions, but without Y151D (R3 and R12). This behavior is not surprising for two reasons. First, K41D is a basic to acidic substitution, while Y151D is a polar to acidic substitution and therefore the change in overall basicity near the cysteine

residues due to the Y151D substitution would be less than for K41D. Second, in the R8 model, residue 41 is closer to Cys204 (9.3 Å, Cα–Cα distance, see Chapter 3) than is residue 151 (14.4 Å), reducing the influence of the acidic substitution relative to K41D.

Oxidative midpoint potentials were measured for each of the mutants to determine the degree to which the thermodynamic stabilities of the disulfide bonds were affected by the substitutions. Midpoints varied only by 21 mV, from  $E^{\circ'} = -284$  to  $-263$  mV (R8 and R14, respectively). However, rate constant and midpoint potential correlated well (correlation coefficient = 0.84) with the faster mutants having more oxidizing midpoints.

The determining factors of the thermodynamic stability of a disulfide bond (i.e. midpoint potential) and their relative contributions are not well understood. Research to date has focused on two general groups of factors as important determinants: (1) electrostatic influence on thiol ionizability (discussed below) and, (2) geometric strain considerations (discussed in Chapter 3).

Lower thiol  $pK_a$  in a disulfide cysteine leads to a more stable thiolate, and thus, a more reactive side chain and, in general, a less stable disulfide (Creighton 1975; Nelson and Creighton 1994). The relationship between midpoint potential and thiol ionizability has been studied in the thiol:disulfide oxidoreductase family of enzymes. This family includes enzymes that catalyze the formation, isomerization, and removal of disulfide bonds in proteins through a characteristic active site motif

Cys-X-X-Cys (where “X” is any amino acid) in the thioredoxin fold (Martin 1995). While the disulfide bond that forms between the active-site cysteine residues is conformationally very similar among members of this family,  $E^{\circ'}$  vary considerably, from  $-122$  mV for DsbA, to  $-270$  mV for thioredoxin 1 (Aslund and Beckwith 1999). The  $pK_a$  of the surface-exposed catalytic cysteine of DsbA is considerably more acidic (3.5) than that of thioredoxin (6.7) and the large differences in midpoint potential between these enzymes with superimposable active sites (Martin et al. 1993) have been attributed to differential electrostatic stabilization of the cysteine thiolate (Gane et al. 1995; Grauschopf et al. 1995). This trend of more acidic disulfide cysteines leading to less stable disulfides (i.e. less negative midpoint potential) is also seen with the roGFP mutants.

### Materials and Methods

Rate-enhanced roGFP mutants (roGFP-R mutants) were designed based on the concept that disulfide formation proceeds preferentially through the thiolate anion of one of the cysteines (Lindley 1960). The placement of positively charged residues near a cysteine would be expected to lower its thiol  $pK_a$  and thus increase the rates of disulfide formation and breakage. Three surface-exposed sites near the roGFP disulfide were selected for mutation by visual inspection of the atomic model of

roGFP2 (Hanson et al. 2004) and S65T GFP (Ormo et al. 1996) (PDB codes 1JC1 and 1EMA, respectively). Model-building suggested that a basic substitution at position 149, 202, or 223 might reasonably result in an electrostatic interaction with the disulfide cysteines. In the first round of mutagenesis three single mutants of roGFP1 (GFP with C48S/S147C/Q204C) were constructed by site-directed mutagenesis of each site to lysine or arginine. Subsequent rounds of mutagenesis added additional charged groups for a total of nine variants with 1–4 amino acid positions replaced with lysine, arginine, or aspartate (see Table 1 for nomenclature). Aspartate was included to investigate the role of the Cys-Arg-Asp catalytic triad found in some redox-sensitive enzymes.

### **Gene construction and protein expression/purification**

Mutations were introduced using a version of the QuickChange (Stratagene) protocol that allows multiple amino acid substitutions in the same round of mutagenesis using a single primer for each mutation (Sawano and Miyawaki 2000). DNA sequencing of the entire GFP coding region verified each mutation. Mutations were introduced into a His-tagged version of roGFP1 (with Q80R) in the plasmid pRSET<sub>B</sub>.

Mutant protein was expressed in *E. coli* strain JM109(DE3) using the pRSET<sub>B</sub> expression system with an N-terminal His<sub>6</sub> tag and grown to an OD<sub>600</sub> of 0.8 at 37° in a 4-liter fermenter. IPTG was added and cells were allowed to induce overnight at

18°. Cells were pelleted by centrifugation and then resuspended in 50 mM HEPES (pH 7.9), 300 mM NaCl, 10% glycerol and then sonicated for five minutes. Cell lysate was centrifuged and the supernatant was applied to a column of  $\text{Ni}^{2+}$ -nitrilotriacetic acid agarose resin (Qiagen) for purification. Because GFP is quite resistant to protease degradation, incubation with 2% (w/w)  $\alpha$ -chymotrypsin (20 hours, room temperature) was used to cleave the His-tag and further remove protein impurities. Samples were concentrated by filtration (Centrion 30; Amicon) and buffer-exchanged with PD-10 Sephadex columns (Amersham Biosciences) into 50 mM HEPES (pH 7.9) with 300 mM NaCl.

### **Ratiometric fluorescence measurements**

RoGFP1 (and its mutants) displays two fluorescence excitation maxima at 395 and 475 nm, with emission measured at 510 nm, and the relative amplitudes are directly related to the oxidation state of the protein (Hanson et al. 2004). Since this behavior is ratiometric with a clear isosbestic point, the ratio of the intensities of these peaks can be used to measure redox state independent of protein concentration, sample path length, photobleaching and variable source intensity (Gryniewicz et al. 1985). Fluorescence measurements were made on a PerkinElmer Lifesciences LS55 fluorescence spectrophotometer.

### Determination of quantum yield

Fluorescence quantum yields were determined for roGFP1 and each of the nine new mutants. Samples of protein were prepared so that 400-nm absorbance was equal to that of a 9-aminoacridine ( $\lambda_{\text{max, abs}} = 400 \text{ nm}$ ) standard dissolved in water. Total emission with excitation at 400 nm was measured and quantum yields were determined from the total emission ratios using the accepted values for the dye standard ( $\Phi_F = 0.98$  for 9-aminoacridine (Weber and Teale 1957)). Emission spectra were corrected for wavelength-dependent photomultiplier sensitivity using the manufacturer-supplied correction curves and integrated using the supplied software (FL Winlab). As a control, the quantum yield ( $\lambda_{\text{ex}} = 400 \text{ nm}$ ) of wild-type GFP was determined using the same method and was found to be 0.78. This is in good agreement with values previously reported in the literature (Patterson et al. 1997).

### Rate determinations

In vitro rates for the reaction of roGFP1 and its variants with DTT and  $\text{H}_2\text{O}_2$  were determined at low salt concentration by monitoring the fluorescence excitation ratio over time after the addition of a large excess of reagent. All solutions were degassed before use and buffers were then bubbled with nitrogen to remove any remaining dissolved molecular oxygen. Experiments were carried out at  $25^\circ$  in disposable 2-mL cuvettes with around  $0.5 \mu\text{M}$  protein ( $0.01 \text{ mg/mL}$ ). Reaction buffer was 50 mM HEPES pH 7.0 with 1 mM EDTA. For  $\text{H}_2\text{O}_2$  experiments, samples were

first diluted from a storage concentration of 1.0–0.1 mM to about 10  $\mu$ M in 20  $\mu$ L of reaction buffer and then incubated at room temperature for 60 minutes with 1 mM DTT to ensure reduction of the disulfide. Samples were diluted in disposable cuvettes to 2 mL with 50 mM HEPES, pH 7.0. Fluorescence excitation was measured every 10–20 seconds after the addition of 1 mM DTT or H<sub>2</sub>O<sub>2</sub>. This was repeated at least twice for each mutant. The fraction of roGFP reduced was calculated from the ratio of excitation peaks using eq 1:

$$R = (F - F_{\text{ox}})/(F_{\text{red}} - F_{\text{ox}}) \quad (1)$$

here,  $R$  is the fraction of roGFP reduced;  $F$  is the fluorescence intensity ratio of the two strongest excitation peaks, at 475 nm and 395 nm; and  $F_{\text{ox}}$  and  $F_{\text{red}}$  are the ratios for the completely oxidized and completely reduced protein, respectively. The pseudo-first-order rate constant for the reaction was determined using a curve fit to eq 2 and is independent of protein concentration:

$$R = A(1 - e^{-kt}) + B \quad (2)$$

here,  $A$  and  $B$  are constants,  $k$  is the first-order rate constant, and  $t$  is time. To determine the effect of salt concentration the DTT reduction rate constants for the variants were determined in 50 mM HEPES, pH 7.0, with 0, 50, 100, 200, or 300 mM NaCl.

### Midpoint determinations

Samples of all variants were prepared at 1  $\mu\text{M}$  in 100 mM HEPES, pH 7.0, with 1 mM total DTT (mixture of oxidized and reduced forms) in 2-mL cuvettes and allowed to incubate for 3–4 hours at 25°. To minimize air-oxidation, all buffers and solutions were degassed and all samples were prepared and incubated in an anaerobic glove-box. After incubation, cuvettes were capped and removed from the glove-box for fluorescence excitation measurements. Apparent redox midpoint potentials for all roGFP1 variants were determined from the equilibrium constant for the reduction of roGFP with DTT. This is determined by measuring the fraction of roGFP reduced ( $R$ , using fluorescence excitation ratios as explained above) at known concentrations of  $\text{DTT}_{\text{ox}}$  and  $\text{DTT}_{\text{red}}$  and plotting  $R$  vs.  $[\text{DTT}_{\text{red}}]/[\text{DTT}_{\text{ox}}]$ , then fitting to a titration curve (see Figure 12) according eq 3:

$$R = ([\text{DTT}_{\text{red}}]/[\text{DTT}_{\text{ox}}]) / (K_{\text{eq}} + [\text{DTT}_{\text{red}}]/[\text{DTT}_{\text{ox}}]) \quad (3)$$

The midpoint potential can then be determined from the Nernst equation (eq 4) where  $R$  is the gas constant ( $8.315 \text{ J K}^{-1} \text{ mol}^{-1}$ ),  $T$  is the absolute temperature,  $n$  is the number of transferred electrons, and  $F$  is the Faraday constant ( $9.649 \times 10^4 \text{ C mol}^{-1}$ ).

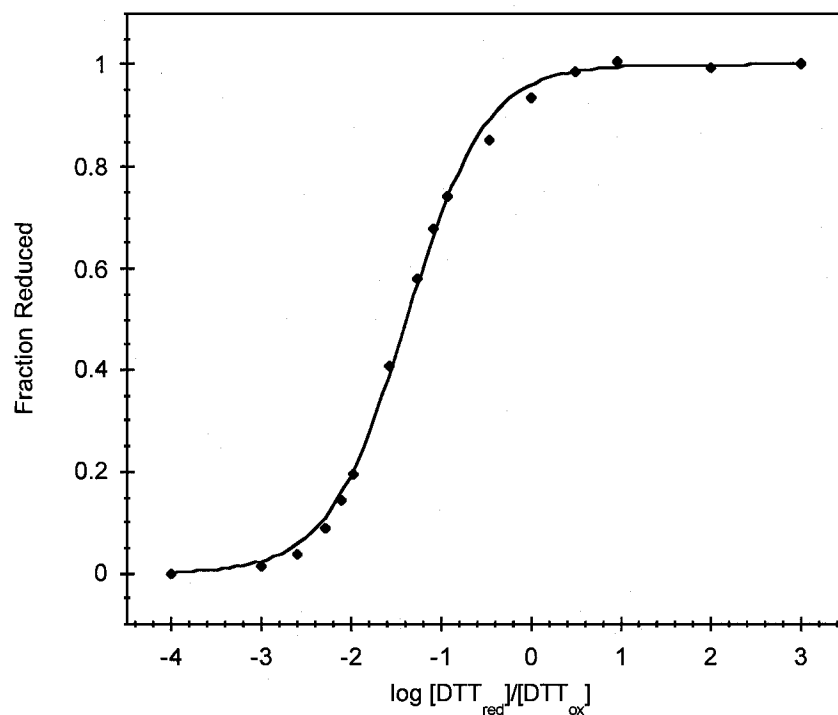
$$E'_{0(\text{roGFP})} = E'_{0(\text{DTT})} - (RT/nF) \ln K_{\text{eq}} \quad (4)$$

As a check, the midpoint potential of roGFP1 was verified using lipoic acid (10 mM total). Plots and curve fits were made using KaleidaGraph (Abelbeck Software).

Midpoint potentials at pH 7.0 and 25° were assumed to be  $E^{\circ}_{(\text{Lip})} = -0.270 \text{ V}$  (Lees and Whitesides 1993) and  $E^{\circ}_{(\text{DTT})} = -0.323 \text{ V}$  (Szajewski and Whitesides 1980).



Figure 12. DTT buffer composition vs. fraction of protein reduced. The  $K_{eq}$  of the reaction of roGFP with DTT was determined by fitting data, such as that shown here, to Equation 3. Fraction reduced is determined from the fluorescence excitation ratio at various ratios of  $DTT_{red}$  to  $DTT_{ox}$ .



### CHAPTER III. RE-ENGINEERING roGFP: STRUCTURAL STUDIES

#### Summary

In order to further understand the roles of the basic substitutions on the ionizability of the engineered cysteine residues and the thermodynamic stability of the disulfide bond, X-ray crystal structures were solved for two of the roGFP1-R mutants. The R7 mutant has two basic substitutions near the disulfide and was crystallized in the oxidized form. R7 crystals diffracted to 2.2 Å and have two molecules per asymmetric unit. The structure shows that the disulfide forms with full occupancy and both basic substitutions are clearly visible in the electron density map. Because there were two mutants, R8 and R10, with basic substitutions that did not show improved response times, the crystal structure of R8 was solved to investigate the structural basis for this behavior. The R8 mutant has one basic and one acidic substitution and was crystallized in the reduced form. R8 crystals diffracted to 1.95 Å

and also have two molecules per asymmetric unit. The electron density map of R8 shows that the cysteine residues are fully reduced and that the two substitutions form a salt-bridge.

Using the refined models of the R7 and R8 structures, electrostatics calculations were performed using solutions to the Poisson–Boltzmann equation to predict the influence of the charged substitutions on the ionizability of the engineered cysteine residues. Predicted cysteine pKa's were used to calculate rate differences over a range of ionic strengths, and these calculated rate differences correlated well with those observed in Chapter 2.

## Results

### **Crystal structure analysis of R7**

The R7 mutant (roGFP1–S202K/F223R) crystals have space group  $P3_221$ , with two molecules per asymmetric unit and diffracted to 2.2 Å resolution using a conventional rotating anode X-ray source. The structure was solved by molecular replacement using the GFP S65T (Ormo et al. 1996)(Protein Data Bank code 1EMA) structure as search model. Refinement was performed without imposing noncrystallographic symmetry restraints, and thus the two molecules in the

asymmetric unit provide independent views of the protein in unique crystal-packing environments. Final model statistics are presented in Table 3.

The two molecules in the asymmetric unit form a different dimer from that seen for either wild-type GFP (Yang et al. 1996) or roGFP2 (Hanson et al. 2004). With the A molecules of R7 and wild-type GFP aligned, a rotation of  $-82.8^\circ$  and translation of 0.3 Å aligns the B molecule of R7 on wild-type GFP (see Figure 13). The ordered C-terminus of R7 (see below) and the mutation of several of the wild-type residues (S147C, Q204C, S202K, and F223R) involved in the wild-type GFP dimer disallow the formation of the same dimer in R7. Table 4 compares the dimer contacts for R7, R8 and wild-type GFP. The disulfides of both R7 molecules are positioned adjacent to each other in the middle of the dimer contact about 4 Å apart; however, there is no evidence for intermolecular disulfide formation. Several specific electrostatic interactions between the A and B molecules, as well as stacking of the Tyr237 phenol rings, and a larger buried surface area than that seen with the wild-type GFP dimer or the roGFP2 dimer ( $2,008 \text{ Å}^2$  compared to  $1,772 \text{ Å}^2$  or  $1,403 \text{ Å}^2$  respectively, determined using the program EDPDB (Zhang and Matthews 1995)) may indicate some relevancy in solution. However, ultracentrifugation experiments showed that the R7 protein is a monomer in solution at concentrations less than 1 mM (data not shown).

The cysteine residues 147 and 204 form a disulfide with full occupancy in both protomers comprising the asymmetric unit. This disulfide shares the  $\text{pg}^- \text{g}^-$

Table 3.

Data collection and refinement statistics for oxidized R7 and reduced R8		
Data collection	R7 (oxidized)	R8 (reduced)
Crystal		
Total observations	272,860	473,006
Unique reflections	36,457	45,355
Cell dimensions (a, b, c) (Å)	126.3, 126.3, 78.4	79.7, 79.7, 166.9
Resolution (Å)	40.0-2.20	50.0-1.95
Highest resolution shell (Å)	2.28-2.20	2.02-1.95
Completeness <sup>a</sup> (%)	99.9 (100)	99.5 (99.9)
Multiplicity <sup>a</sup>	7.48	10.4
Average $I/\sigma$ <sup>a</sup>	21.6 (2.6)	50.7 (8.8)
$R_{\text{merge}}$ <sup>a,b</sup>	0.096 (0.634)	0.141 (0.483)
Refinement		
Space group	P3 <sub>2</sub> 21	P3 <sub>2</sub> 21
No. of molecules <sup>c</sup>	2	2
No. of protein atoms <sup>c</sup>	3,544	3,456
No. of solvent atoms <sup>c</sup>	164	211
Resolution range (Å)	24.0-2.20	50.0-1.95
Crystallographic $R$ -factor <sup>d</sup> (reflections)	0.196 (32,733)	0.199 (40,816)
$R$ -free (reflections)	0.289 (3,722)	0.275 (4,530)
combined	0.204	0.204
Average $B$ -factors (Å <sup>2</sup> )		
Protein atoms (main chain)	44.9	36.4
Solvent	46.9	47.3
Root mean square deviations from ideality		
Bond lengths (Å)	0.017	0.013
Bond angles (degrees)	3.0	2.6
$B$ -factor correlations (Å <sup>2</sup> )	5.9	4.1

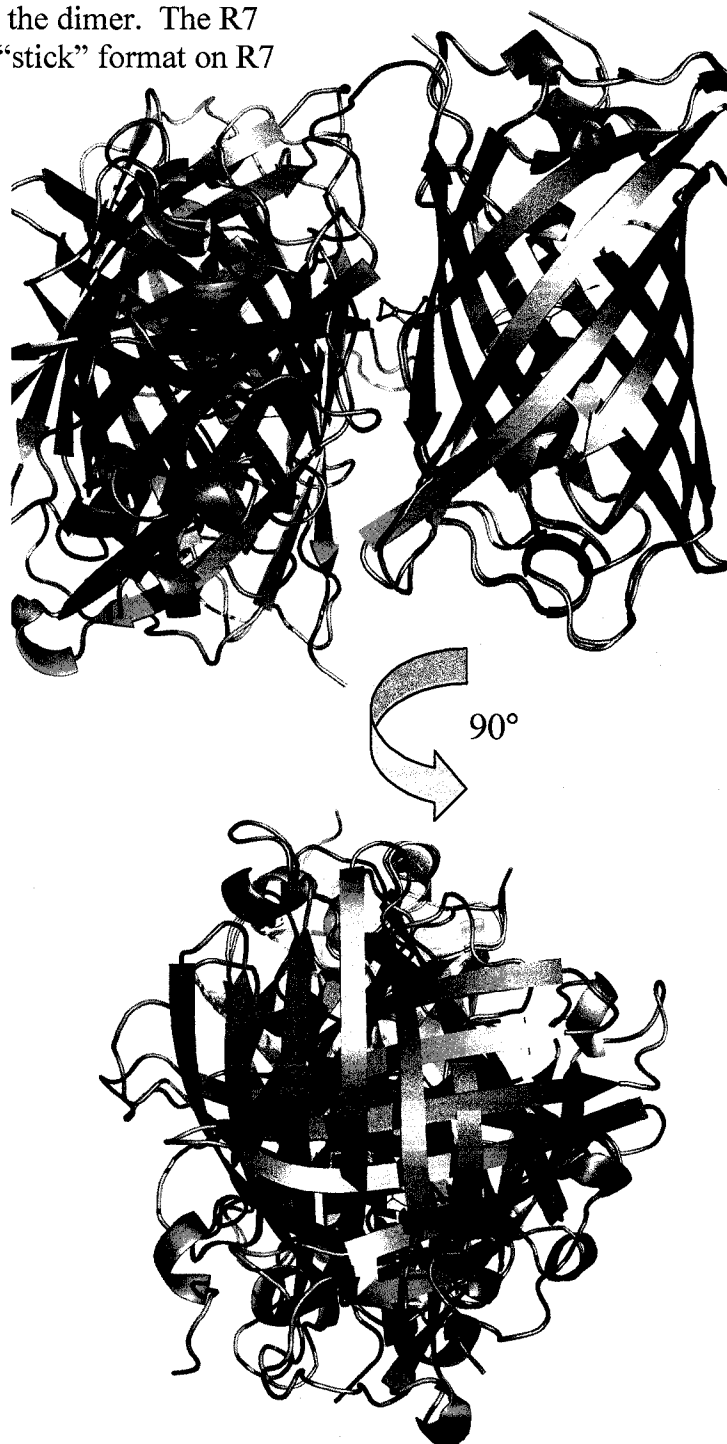
<sup>a</sup> Values in parentheses indicate statistics for the highest resolution shell.

<sup>b</sup>  $R_{\text{merge}} = \sum I <I> / \sum <I>$ , where  $I$  is the observed intensity, and  $<I>$  is the average of intensities obtained from multiple observations of symmetry-related reflections.

<sup>c</sup> Per asymmetric unit.

<sup>d</sup>  $R$ -factor =  $\sum ||F_o| - |F_c|| / \sum |F_o|$ , where  $F_o$  and  $F_c$  are the observed and calculated structure amplitudes, respectively.

Figure 13. An alignment of the A-molecules of R7 and wild-type GFP. R7 is shown in green and wild-type GFP in cyan. The 90° rotated image (lower image) shows the differing configurations of the B-molecules in the dimer. The R7 disulfide is shown in “stick” format on R7 molecule A.



conformation with the disulfides found in the oxidized structure of roGFP2 (Protein Data Bank code 1JC1; roGFP2 is roGFP1 with the internal chromophore substitution S65T), solved previously (Hanson et al. 2004). The descriptive parameters for the disulfides, with the value for the A-protomer given first, are as follows:  $\chi^1_{147}$  angle of  $-49.4^\circ$ ,  $-60.0^\circ$ ;  $\chi^1_{204}$  angle of  $-61.8^\circ$ ,  $-48.8^\circ$ ;  $\chi^2_{147}$  angle of  $-112.9^\circ$ ,  $-101.3^\circ$ ;  $\chi^2_{204}$  angle of  $-67.7^\circ$ ,  $-90.5^\circ$ ;  $\chi_{ss}$  angle of  $101.5^\circ$ ,  $107.6^\circ$ ; C $\alpha$ –C $\alpha$  distance of 4.06 Å, 4.06 Å; and C $\beta$ –C $\beta$  distance of 4.11 Å, 4.06 Å. These values do not deviate significantly from those seen for the naturally strained disulfides occasionally found between adjacent antiparallel  $\beta$ -strands. Srinivasan et al. (Srinivasan et al. 1990) did not present standard deviation values in their very helpful statistical analysis of protein disulfide bond geometries. However, examination of the same 22 PDB files analyzed by Srinivasan et al. reveals that the geometric parameters of both R7 disulfides fall within one standard deviation of the parameters for those disulfides classified as bridging across antiparallel  $\beta$ -strands (Srinivasan et al. 1990). Table 4 compares the disulfide geometry statistics for R7, roGFP2, and for the PDB files analyzed by Srinivasan and coworkers. Compared to the group of all disulfides with a right-handed spiral (positive value for the  $\chi_{ss}$  angle) from the same work, the R7 disulfide  $\chi_{ss}$  angle values are within one standard deviation of the average value of  $96^\circ \pm 15^\circ$ , but the R7 disulfide C $\alpha$ –C $\alpha$  distances are much shorter than the average value of 5.2 Å  $\pm 0.7$  Å for this same group of disulfides (Srinivasan et al. 1990). Although this

Table 4.

## Comparison of dimer contacts.

wtGFP					R7				R8			
A mol. position	A.A. <sup>a</sup>	B mol. contact <sup>b</sup>	% access. monomer <sup>c</sup>	% change in dimer <sup>d</sup>	A.A. <sup>a</sup>	B mol. contact <sup>b</sup>	% access. monomer <sup>c</sup>	% change in dimer <sup>d</sup>	A.A. <sup>a</sup>	B mol. contact <sup>b</sup>	% access. monomer <sup>c</sup>	% change in dimer <sup>d</sup>
34	Glu	-	34	0	Glu	-	33	0	Glu	R223	29	25
39	Tyr	S208	43	28	Tyr	E172	36	22	Tyr	-	38	19
41	Lys	-	19	0	Lys	-	23	8	Asp	E34	20	15
73	Arg	-	28	7	Arg	E142	16	9	Arg	-	26	0
142	Glu	N149	23	13	Glu	-	16	8	Glu	-	22	0
143	Tyr	-	21	3	Tyr	Y39	21	7	Tyr	-	20	0
145	Tyr	S147	8	5	Tyr	-	7	4	Tyr	-	10	0
146	Asn	-	15	14	Asn	R223	14	13	Asn	-	21	0
147	Ser	Y145	25	25	Cys	L236	19	18	Cys	-	39	25
149	Asn	E142	23	14	Asn	-	15	1	Asn	N212	27	13
168	Arg	-	30	7	Arg	E235	29	16	Arg	-	27	0
172	Glu	-	40	0	Glu	Y39	42	11	Glu	-	40	0
202	Ser	-	18	8	Lys	-	6	0	Ser	N212	18	14
204	Gln	L207	32	29	Cys	-	12	6	Cys	-	25	24
207	Leu	Q204	8	7	Leu	-	8	0	Leu	-	9	4
208	Ser	Y39	25	20	Ser	-	24	7	Ser	C204	23	21
209	Lys	-	30	4	Lys	-	29	0	Lys	C204	29	7
223	Phe	-	24	22	Arg	N146	26	20	Arg	E34	34	23
233	Met	-	-	-	Met	R168	59	28	Met	-	-	-
235	Glu	-	-	-	Glu	R168	11	6	Glu	-	-	-
236	Leu	-	-	-	Leu	C147	17	15	Leu	-	-	-
total buried surface area, dimer (Å <sup>2</sup> ): <sup>e</sup>				1804	2057				2050			
% of total dimer surface area:				8.5	10.1				10.5			

<sup>a</sup> Amino acid identity, mutations are in red.<sup>b</sup> Contact was defined as an interaction (sidechain or backbone) of < 3.2 Å between potential H-bond donor/acceptor pairs.<sup>c</sup> The % of total residue surface area buried by intramolecular contacts.<sup>d</sup> The % decrease in solvent exposed surface area due to dimer contacts.<sup>e</sup> Accessible surface areas were all calculated using EdPDB (Zhang, 1995) with the 1GFL (Yang, 1996), R7 and R8 PDB files.



is evidence for some strain on the R7 disulfides they are less strained than those found in the roGFP2 crystal structure, where the average  $\chi_{ss}$  angle is  $116^\circ$  (Hanson et al. 2004).

The two R7 surface mutations, S202K and F223R, are clearly defined by the electron density map. The side chains of these two residues are oriented away from the disulfide, with the charged groups located about 8 Å from the disulfide sulfur atoms (see Figure 14).

A unique characteristic of the oxidized R7 structure is that the C-terminal residues (230–238) are ordered. They form a short  $\beta$ -strand that lies along the outside surface of the  $\beta$ -barrel and terminates quite near the position of the engineered disulfide. Several specific interactions between this C-terminal strand and the  $\beta$ -barrel surface suggest that this is likely not just an artifact of crystal packing. These interactions include hydrogen bonds between the  $O\epsilon_1$  of Glu235 and the  $N\zeta$  of Lys202, between the phenol hydroxyl of Tyr237 and both  $N\delta$  of Asn149 and the backbone oxygen of His148, as well as non-polar interaction between Leu236 and the disulfide. This places the last four residues of the C-terminus very close to the disulfide environment so that the side chain of Leu236 is oriented between Arg223 and the disulfide and so that the phenol of Tyr237 is between Lys202 and the disulfide (see Figure 15).

Figure 14. The “active-site” of R7, showing the disulfide and basic substitutions (S202K and F223R) in “stick” format. The uniquely ordered C-terminal tail is colored cyan, and C-terminal residues that are near the disulfide are shown in stick format. Residues before and after the disulfide cysteines are also in stick format to better show their positions. Dashed lines are labeled with distances between the sulfur of Cys204 and the basic ends of the substitutions.

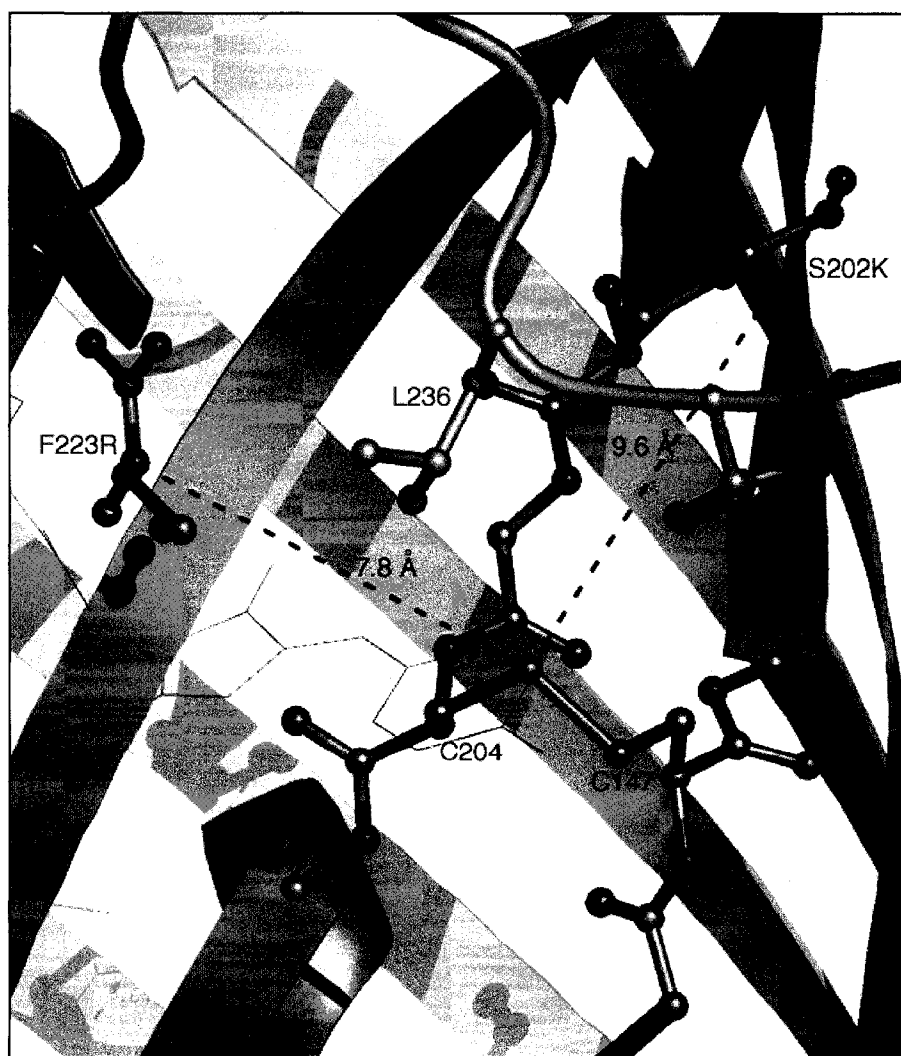


Figure 15. Stereo image of R7. The C-terminal residues contacting the surface substitutions are shown in blue.



### Crystal structure analysis of R8

Two variants (R8 and R10) contain additional basic residues near the disulfide but did not show increased disulfide reduction rates compared to roGFP1, possibly because each carries the substitution K41D. Crystals of reduced R8 (roGFP1–F223R/K41D) have space group  $P3_121$  and diffracted to 1.95 Å on APS beamline 14BM–C. The structure was solved by molecular replacement in a similar manner to the oxidized R7 structure.

As expected, the electron density map of R8 shows no evidence for a disulfide bond between cysteines 147 and 204. The C $\alpha$ –C $\alpha$  distance between Cys147 and Cys204 is 4.6 Å, compared to a distance of 4.0 Å in the oxidized R7 structure. An overlay of the R7 and R8 models (see Figure 16) shows that the R8 Cys204 backbone is clearly shifted away from Cys147 compared to R7, while the position of Cys147 remains essentially the same, as observed for roGFP2 (Hanson et al. 2004). There is no evidence of further cysteine oxidation by oxygen or crosslinks with other molecules to Cys147 or Cys204 in either of the two molecules in the asymmetric unit.

Asp41 and Arg223 form a salt-bridge. The distance between the O $\delta_1$  of Asp41 and the N $\epsilon$  of Arg223 is 2.8 Å in both molecules (see Figure 17). This electrostatic interaction clearly reduces the effect of Arg223 on the pK $_a$  of the Cys204 thiol as the R3 mutant contains the F223R substitution and shows an almost 2-fold rate enhancement over roGFP1, while R8 shows no rate enhancement.

Figure 16. Overlay of R7 and R8 active-sites. R7 is shown in green and R8 in yellow. The  $\beta$ -strand containing Cys147 is shifted away from its neighboring  $\beta$ -strand containing Cys204 in the reduced molecule (R8). This shift was also seen in the reduced/oxidized roGFP2 structures (Hanson et al. 2004).

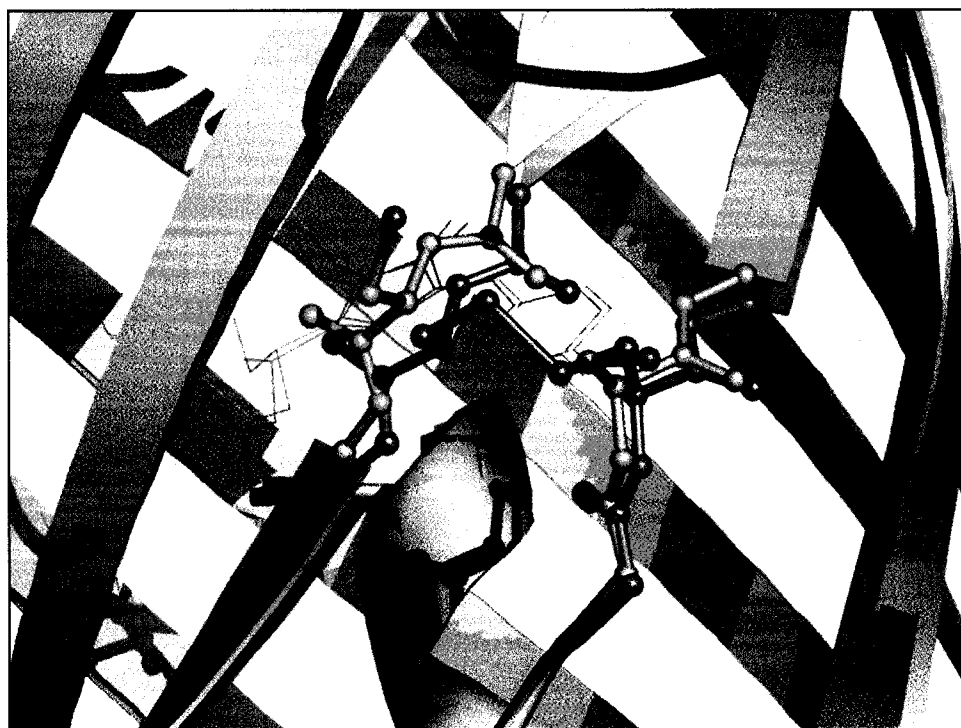
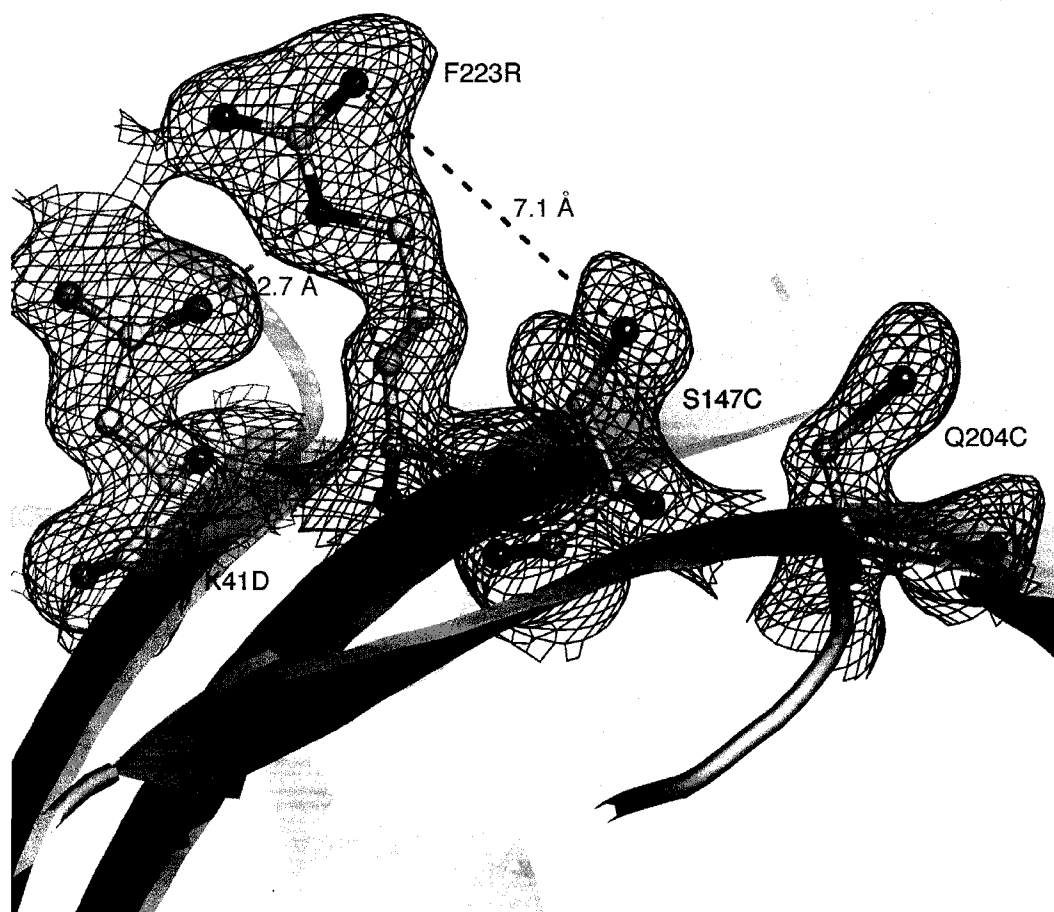


Figure 17. The “active-site” of R8. Substitutions are shown in “stick” format with electron density ( $2F_o - F_c$ ,  $\sigma = 1.0$ ) within 2 Å of the residues displayed as wire mesh.



The asymmetric unit of the R8 crystals contains a protein dimer different from that of either R7 or wild-type GFP (see Table 5). The backbone oxygen of Lys209 is positioned between the thiols of Cys147 and Cys204 of the neighboring molecule, with Lys209 O an average of 3.5 Å away from the cysteine sulfur atoms. With the A-molecules of R8 and wild-type GFP aligned, a rotation of 79.1° and translation of 3.5 Å aligns the B-molecule of R8 with wild-type GFP.

An attempt was made to produce oxidized crystals of R8 by transferring the reduced crystals to a solution without DTT. The crystals survived this process and diffracted well a week after being transferred, however the electron density map showed no evidence of disulfide formation. A similar result occurred when attempting to produce a reduced form of R7 from the oxidized crystals, therefore the tight dimer interface formed at the cysteine positions seems to preclude the easy modification of the cysteine redox status.

### **Electrostatics Calculations**

To further test the theory that the observed rate enhancements on the roGFP1-R mutants are due to the introduced basic residues decreasing the pK<sub>a</sub>'s of Cys147 and/or Cys204 through electrostatic interactions, the program DelPhi (Rocchia et al. 2001; Rocchia et al. 2002) was employed to provide solutions to the non-linear Poisson–Boltzmann equation for mutants R7 and R8. The change in pK<sub>a</sub> expected from addition of the charged substitutions was calculated from the change in site

Table 5.

<i>Comparison of disulfide torsion angles</i>						
	$\chi_{ss}$	$\chi_1^1$	$\chi_2^1$	$\chi_1^2$	$\chi_2^2$	C $\alpha$ -C $\alpha$
Population <sup>a</sup> ave	95	-66	-63	-73	-68	4.54
population stdev	10.9	11.1	13.0	17.1	16.5	0.31
roGFP2 <sup>b</sup> ave	116 <sup>d</sup>	-66	-63	-100	-79	4.04
R7 ave	105	-55	-55	-107	-79	4.06
SRH <sup>c</sup> ave	106	62	-27	-97	-108	4.36
SRH stdev	5.0	5.9	54.1	19.4	31.7	0.42
roGFP2 ave	116	-66	-63	-100	-79	4.04
R7 ave	105	-55	-55	-107	-79	4.06

<sup>a</sup> Average torsion angles for the population in which the roGFP disulfide would fall. The distribution for each torsion angle can easily be broken up into three or four discrete populations separated by at least 20°, C $\alpha$ -C $\alpha$  distance distribution is divided into three populations of small (3.8-4.8 Å), medium (4.8-5.8 Å) and large (>5.8 Å).

<sup>b</sup> RoGFP2 torsion angles from PDB file 1JC1 (Hanson et al. 2004).

<sup>c</sup> SRH is the group of five disulfides defined by Srinivasan et al. as bridging across anti-parallel  $\beta$ -strands (Srinivasan et al. 1990).

<sup>d</sup> Torsion angle values in red are more than one standard deviation removed from the population average.



potential at positions 147 and 204 of the R7 and R8 crystal structures (using A-molecules only) with and without charged substitutions (see Materials & Methods). Since the C-terminal end of the R7 mutant partially buries Cys147 and Cys204 as well as the site of the S202K substitution in the oxidized R7 crystal structure,  $\Delta pK_a$  changes were also calculated for R7 with the residues 230–238 deleted, since the C-terminus may be disordered in solution (as it is in other GFP structures). From these calculated  $\Delta pK_a$ 's rate enhancements over parent roGFP1 were calculated based on the assumption that the reaction mechanism is pH-dependent. These calculated rate enhancements are compared to those observed experimentally over a range of ionic strengths in Table 6 and are plotted in Figures 18 and 19. Both plots are linear over the range of ionic strengths tested, indicating a strong correlation between theory and experiment. Reaction rates were calculated assuming that either Cys147 or Cys204 formed the reactive thiolate. Experimentally, R8 was observed to have a faster  $k_{DTT}$  at higher ionic strengths, and this is correctly predicted by the calculations. In each case Cys204 is predicted to have a larger  $\Delta pK_a$  than Cys147 due to the charged substitutions, however, this is not surprising since the basic substitutions are located closer to Cys204 than Cys147.

Table 6.

*Calculated vs. Experimental Rate Enhancements*

R8

ionic strength	calc. $\Delta pK_a$		calc. rate enhancements			experimental rate enhancements <sup>a</sup>
	C147	C204	C147	C204	ave.	
50	0.033	0.074	0.928	0.844	0.886	0.857
100	0.020	0.054	0.954	0.883	0.919	0.886
150	0.015	0.043	0.967	0.905	0.936	0.873
250	0.009	0.032	0.979	0.929	0.954	0.924
350	0.007	0.025	0.984	0.943	0.964	0.928
mM	cc: <sup>b</sup>		0.884	0.907	0.899	

R7

ionic strength	calc. $\Delta pK_a$		calc. rate enhancements			experimental rate enhancements <sup>a</sup>
	C147	C204	C147	C204	ave.	
50	-0.426	-0.656	2.666	4.525	3.595	3.107
100	-0.366	-0.593	2.323	3.918	3.120	2.402
150	-0.333	-0.558	2.154	3.613	2.883	1.975
250	-0.295	-0.515	1.971	3.277	2.624	1.768
350	-0.271	-0.489	1.868	3.083	2.475	1.630
mM	cc: <sup>b</sup>		0.992	0.991	0.991	

## R7 - C-terminal residues removed

ionic strength	calc. $\Delta pK_a$		calc. rate enhancements			experimental rate enhancements <sup>a</sup>
	C147	C204	C147	C204	ave.	
50	-0.421	-0.596	2.636	3.947	3.291	3.107
100	-0.346	-0.511	2.217	3.246	2.731	2.402
150	-0.304	-0.463	2.014	2.901	2.458	1.975
250	-0.255	-0.403	1.798	2.531	2.164	1.768
350	-0.224	-0.365	1.677	2.319	1.998	1.630
mM	cc: <sup>b</sup>		0.993	0.992	0.992	

<sup>a</sup> from comparison of roGFP1 and R7 or R8 rate constants determined by adding 1 mM DTT to oxidized protein in 50 mM HEPES pH 7.0 with [NaCl] = 0-300 mM (see materials & methods).

<sup>b</sup> correlation coefficient of calculated to experimental rate enhancements

Figure 18. Calculated vs. experimentally observed rate enhancements for R7 (compared with rates for roGFP1) over a range of ionic strengths. Calculations were done using solutions to the Poisson–Boltzmann equation on the R7 model with and without the 8 C-terminal residues. The slopes of the linear fit and correlation coefficients (R) are listed. Data for Cys204 shows the slope closest to one.

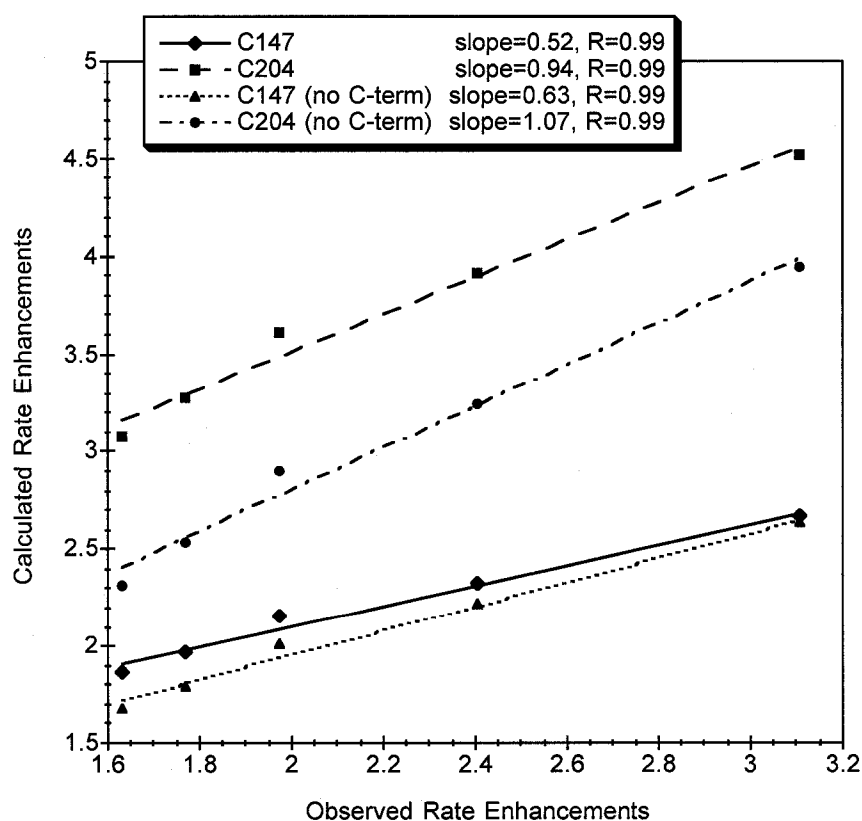
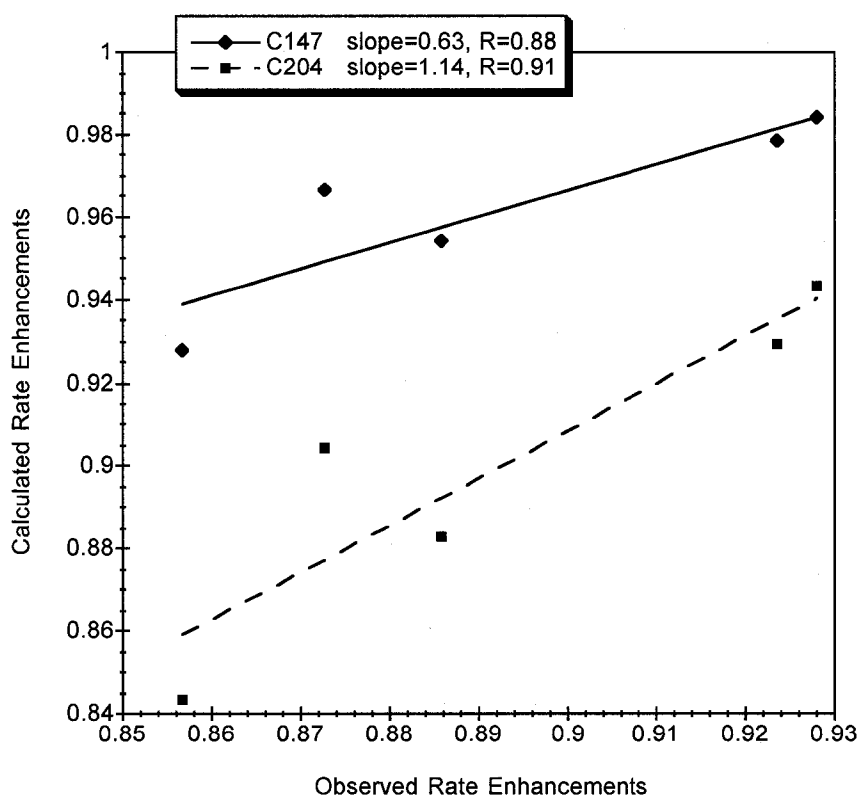


Figure 19. Calculated vs. experimentally observed rate enhancements for R8 (compared with rates for roGFP1) over a range of ionic strengths. The slopes of the linear fit and correlation coefficients (R) are listed. Data for Cys204 again shows the slope closest to one.



## Discussion

### **Rate enhancements**

In the R7 model the basic substitutions at positions 202 and 223 are clearly visible in the vicinity of the disulfide, but are not within hydrogen bond distance of either of the cysteines. In the crystal, the ordered C-terminal residues and segments from the adjacent molecule contact the disulfide, possibly forcing residues 202 and 223 away from the cysteines. Calculations were performed using solutions to the Poisson–Boltzmann equation to predict the electrostatic contributions from the introduced basic residues on the pK<sub>a</sub>'s of the reactive cysteines. The rate enhancements predicted from these calculations linearly followed the experimentally observed rate enhancements for R7. However, calculations in the presence and absence of the eight C-terminal residues yielded similar results, suggesting that these contacts are irrelevant in solution. Nevertheless, it was shown that the basic substitutions, in their observed positions, make a significant electrostatic contribution to the cysteine pK<sub>a</sub>s and hence can account for a significant component of the observed rate enhancements.

The roGFP1 mutants with the substitution K41D (R8 and R10) had significantly reduced rate enhancements over roGFP1 compared to the same mutants without K41D, and, unlike the other mutants, had increasing rates with increasing salt concentrations. This behavior was successfully modeled by DelPhi for the R8

mutant. In the reduced R8 structure, a salt-bridge is formed between the side chains of K41D and F223R, but this does not increase the distance between the guanidinium group and cysteine sulfurs compared to the R7 model without K41D. The contribution of the K41D substitution to the  $pK_a$  of the cysteines, therefore, is more likely a function of its basic substitution being next to an acidic substitution and thus electrostatically minimized, than because of a conformational restriction imposed on F223R by the salt-bridge.

### Midpoint potential

The family of oxidoreductases has been used to study the various factors influencing disulfide stability in proteins (discussed in Chapter 2). The correlation of cysteine thiol  $pK_a$  with  $E^\circ$  may explain the midpoint differences between the two oxidoreductases with most widely differing midpoint potentials, DsbA and thioredoxin; however, cysteine  $pK_a$  differences alone cannot fully explain the  $E^\circ$  differences between all members of the oxidoreductase family and subtle differences in tertiary structure probably also play an important role (Chivers et al. 1997; Moutevelis and Warwicker 2004). Using small molecule dithiols that formed rings upon disulfide formation, Burns et al. showed that higher geometric strain corresponded to lower disulfide stability (Burns and Whitesides 1990). Higher geometric strain also leads to less stable disulfides in proteins (Katz and Kosiakoff 1986; Wells and Powers 1986). Disulfides bridging across antiparallel  $\beta$ -strands are

relatively rare in proteins and the disulfide geometry imposed by this conformation leads to a characteristically strained bond (Hogg 2003). Unsurprisingly, therefore, a comparison of the disulfide geometry of roGFP2 with other disulfides found in the protein data bank implies that the roGFP2 disulfide is quite strained. Surprisingly, however, this bond is very stable with  $E^{\circ'}_{\text{roGFP2}} = -272$  mV (Hanson et al. 2004), indicating that it is just as reducing as the catalytic disulfide in the *E. coli* thiol-reductase thioredoxin. While the geometry of the R7 disulfide appears to be somewhat less strained than that of roGFP2 it is slightly less stable ( $E^{\circ'}_{\text{R7}} = -268$  mV) than roGFP2 or roGFP1 ( $E^{\circ'}_{\text{roGFP1}} = -281$  mV). It is unclear, therefore, what effect geometric strain has on the high stability of the roGFP disulfides.

Fluorescent protein-based redox probes have been developed with more oxidizing midpoints by Østergaard *et al.*, who placed pairs of cysteines on the surface of yellow fluorescent protein (YFP), itself a mutant of *A. victoria* GFP (Ormo et al. 1996), in positions that would allow disulfide formation in oxidizing conditions (Østergaard et al. 2001). These probes, designated rxYFP<sup>N</sup><sub>M</sub> (where *N* and *M* indicate the locations of the introduced cysteines) were shown to respond to redox levels with overall (not ratiometric) changes in fluorescence intensity. RxYFP<sup>149</sup><sub>202</sub> was reported to have a midpoint potential somewhat more oxidizing ( $E^{\circ'} = -261$  mV (Østergaard et al. 2001)) than that of the roGFP with the same disulfide pair ( $E^{\circ'}_{\text{roGFP3}} = -299$  mV

(Hanson et al. 2004)). This difference is likely due to subtle differences in disulfide geometry (and measurement technique) since the surface residues near the disulfide are identical in both molecules.

## Materials and Methods

### **Crystal structure determinations**

R7 (roGFP1–S202K/F223R) was concentrated to 40 mg/mL in 50 mM HEPES, pH 7.9, and 300 mM NaCl. Crystals grew in 1–2 days by hanging drop vapor diffusion against 1.1 M Na citrate and 0.1 M imidazole pH 7.6. With normal oxygenated buffer and no reducing agent the protein is completely oxidized, so no disulfide catalyst was necessary. Drops contained 2  $\mu$ L of protein solution and 2  $\mu$ L of well solution. For low-temperature diffraction data collection crystals were transferred to the same well solution plus 15% glycerol.

R8 (roGFP1–K41D/F223R) was concentrated to 32 mg/mL in 50 mM HEPES, pH 7.9, and 300 mM NaCl. Long, hexagonal rod crystals grew overnight by hanging drop vapor diffusion against 1.9 M ammonium sulfate, 0.1 M sodium phosphate/citrate, pH 4.6, and 5 mM DTT. Drops contained 1  $\mu$ L of protein solution and 1  $\mu$ L of well solution. For low-temperature diffraction data collection crystals were transferred to the same well solution plus 20% glycerol.



X-ray diffraction data were collected from a single frozen crystal on an Raxis-IV system for R7 and from a single frozen crystal on APS beamline 14BM-C for R8. Data sets were indexed and reduced using Denzo and Scalepack, or the HKL2000 suite (Otwinowski and Minor 1997). Molecular replacement solutions were found with EPMR (Kissinger et al. 1999), using the GFP S65T coordinate file (Protein Data Bank code 1EMA) as the search model, with positions of amino acid substitution changed to alanines. Positional refinement was initiated using data from 6.0–4.0-Å resolution and then increased in stages to the limit of resolution, using the program TNT (Tronrud et al. 1987). Electron density maps ( $2F_o - F_c$  and  $F_o - F_c$ ) were analyzed and the model rebuilt using the program O (Jones et al. 1991). B-factor refinement was performed using the default TNT B-factor correlation library. Solvent molecules were added only if indicated by large positive features in the ( $F_o - F_c$ ) electron density maps and in reasonable proximity to hydrogen bond partners. In the final rounds of refinement, 100% of diffraction data were used.

### **Electrostatics calculations**

In order to predict cysteine  $pK_a$  differences between roGFP1 and mutants the non-linear form of the Poisson–Boltzmann (PB) equation was solved using finite difference methods with v.4 of the program DelPhi (Rocchia et al. 2001; Rocchia et al. 2002). Differences in the site potential ( $\Delta\Delta G$ ) at the reactive cysteines (Cys147

and Cys204) for the mutants with and without charges at the positions of substitution were used to calculate changes in the cysteine  $pK_a$  through eq 5 (Yang et al. 1993), where  $k$  is the Boltzmann constant:

$$\Delta pK_a = -\Delta\Delta G / (2.3kT) \quad (5)$$

If the reaction mechanism proceeds through the thiolate anion, then a reduction of cysteine  $pK_a$  by 1 unit should lead to a 10-fold increase in the rate constant (if  $pH \ll pK_a$ ). The oxidized R7 and reduced R8 models without solvent molecules were used (A-protomers only). Solvent dielectric was set to 80 and protein interior dielectric to 4.0, while an ion exclusion layer of 2.0 Å was specified. The program iteratively solved the nonlinear PB equation until the difference in potential between solutions was less than  $10^{-4}$  kT.  $\Delta\Delta G$  was calculated for the cysteines of both R7 and R8 with substituted residues all uncharged, each individually charged, and finally with all substitutions charged. This was repeated with ionic strength set to 0, 50, 100, 150, 250, 300, and 350 mM. Since the substitution K41D in R8 replaces a basic residue with an acidic residue, potential differences for R8 were determined with either a negative charge at Asp41 or with a positively-charged lysine residue modeled at that site.

## CHAPTER IV. CONCLUSIONS

In order to improve roGFP for use as an intracellular indicator of thiol oxidation status suitable for the study of important transient redox events in cellular systems, roGFP1 was re-engineered to resemble some of nature's highly responsive redox-sensitive enzymes. To this end, charged residues were substituted at positions proximal to the roGFP1 disulfide cysteine residues, creating a total of nine roGFP1 variants (designated R1-R14). By measuring pseudo-first-order rate constants for in vitro reduction or oxidation of these roGFP mutants, it was shown that each basic residue introduced near the disulfide cysteine residues increased the rate of response approximately two-fold over the parent roGFP1. Structural and electrostatic studies on the variants provided evidence for cysteine thiol pK<sub>a</sub>'s reduced by electrostatic stabilization of the thiolate anion. Redox midpoint potentials for these mutants were also determined and while there are not large differences in thermodynamic stability between the mutants, there is a correlation between midpoint and rate constant, with higher rates corresponding to more positive midpoints. This is also evidence for more acidic cysteine pK<sub>a</sub>'s.

Unfortunately, the response times of these new mutants may still be too slow for the measuring of very fast changes in redox potential, including the monitoring of H<sub>2</sub>O<sub>2</sub> bursts produced by many cell-signaling events (Rhee et al. 2000). The approach used here, to model the roGFP disulfide environment around what is seen in enzymes with reactive cysteines by the addition of basic residues, was validated. The re-engineered probes exhibit more rapid responses and are expected to be more useful for in vivo studies. However, because the roGFP disulfide is located on the surface of the GFP  $\beta$ -barrel this approach is limited, as most of these model enzymes have their reactive cysteines in protected pockets within the protein and this would be expected to increase the electrostatic effect of the basic residues on the cysteine sulfhydryl.

### Future Directions

In order to further enhance roGFP response time, a random mutagenesis approach may provide useful information. Randomly mutagenizing the disulfide neighboring residues would be possible using multiple degenerative primers in a similar manner to that used by Sawano, et al. (Sawano and Miyawaki 2000) to develop a mutant of GFP with blue-shifted fluorescence emission. Alternatively, the entire roGFP could be mutagenized using an error-prone PCR method (Cadwell and

Joyce 1994; Camps et al. 2003). Screening could be accomplished by exposing single colonies expressing a randomized roGFP plasmid to small molecule redox reagents that can diffuse into cellular cytosol and react with roGFPs, such as aldrithiol,  $\text{H}_2\text{O}_2$ , or DTT (Dooley et al. 2004). By measuring the fluorescence excitation ratio over time after addition of reagent the fastest colonies could be selected and the enhanced mutants further studied.

The problem of slow response of roGFP was addressed and partly solved, with new roGFP1 variants displaying rate enhancements of almost 7-fold over parent roGFP1; however, the second roGFP1 problem (identified in Chapter 1) of very reducing midpoint potential, remains a concern. The substitutions of basic residues near the disulfide provided a more stabilizing environment for the cysteine thiolates and therefore provided a lower energy barrier for disulfide formation, since the more reactive thiolate anion is necessary for disulfide formation. Mutants with more basic substitutions had more oxidizing (more positive) midpoint potentials, but the difference between the lowest and highest mutant midpoint was only 21 mV. The R14 mutant had the highest (most oxidizing) measured midpoint of any roGFP variant,  $E^{\circ}_{\text{R14}} = -263$  mV. While the ambient redox potential for the cytosol and mitochondria are reducing enough that some population of roGFP can remain in the reduced state within these compartments (Schafer and Buettner 2001; Hanson et al. 2004), in more oxidizing compartments (i.e. the ambient midpoint of the endoplasmic

reticulum has been estimated to be about  $-180$  mV (Hwang et al. 1992; Schafer and Buettner 2001)) any roGFP would be completely oxidized and therefore useless as a redox probe.

Disulfide midpoint potential is determined primarily by the ionizability of the cysteine thiols and the degree of geometric strain in the bond, although there is still much that is unknown about the influencing factors (see discussion sections in Chapter 2 and 3). In order to produce roGFP variants with more oxidizing midpoints it may be possible to re-engineer the structure of the GFP  $\beta$ -barrel to introduce more strain and destabilize the disulfide bond, and to therefore render it more oxidizing. The insertion or deletion of residues on the same  $\beta$ -strand as one of the cysteines might influence geometric strain. Mutagenesis to modify the hydrogen-bonding patterns between  $\beta$ -strands would change the flexibility of the  $\beta$ -barrel and might also allow for disulfides with different stabilities.

Placement of the disulfide forming cysteines at other locations on the protein surface would provide a different amount of strain to a potential disulfide. For example, the crystal structure of the R7 mutant provided evidence for the ordering of the eight C-terminal residues on the surface of the protein at the location of the engineered cysteine residues. A cysteine substitution for one of these C-terminal residues near Cys147 or Cys204 in the R7 model might result in a disulfide bond with very different character. Such a disulfide might not cause any measurable change in fluorescence upon formation, but the additional substitution of an aromatic residue on

the C-terminus could result in energy transfer to the chromophore that would vary with disulfide formation. Østergaard et al. reported an engineered disulfide in YFP (at the positions 202 and 225) with a substantially more oxidizing midpoint potential (Østergaard et al. 2001) than those observed for the positions 147 and 204, or 149 and 202 used in roGFP. Unfortunately, cysteines engineered at these same positions in GFP did not result in a redox-sensitive probe (data not shown).

While the disulfide conformation found in roGFP is rare, there are disulfides found in nature with very similar geometries. For example, in domain 2 (D2) of CD4, a member of the immunoglobulin family of receptors, a strained disulfide is formed between neighboring anti-parallel  $\beta$ -strands of a truncated  $\beta$ -barrel motif (Cys130–Cys159). The reduction of this redox-active disulfide has been shown to be necessary for entry of HIV-1 (Matthias et al. 2002). A comparison of the CD4 D2 disulfide with that of R7 shows that they are superimposable (R.M.S.D. = 0.33 Å for the 12 atoms in the disulfide residues, see Figure 20). While it was the instability of the Cys130–Cys159 disulfide that suggested to researchers that this bond might be redox active and not merely structural (Matthias et al. 2002), the value of its midpoint potential is unknown. A comparison of the midpoint potentials of this (and other, similar disulfides) to that of roGFP2, or R7, would allow the differentiation of geometric factors from the others contributing to the midpoint potential.

RoGFPs are powerful tools for the study of thiol redox chemistry because of the simplicity of observing disulfide bond formation by ratiometric fluorescence

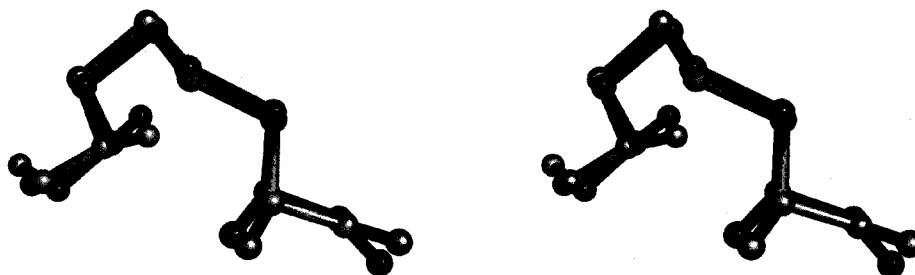


Figure 20. A Stereo image of an overlay of the disulfides of R7 and CD4 D2 (PDB file 3CD4, Cys130–Cys159 disulfide is shown). The R7 disulfide is shown in green and the CD4 disulfide in blue.

measurement. This, combined with the ease of developing new variants by site-directed mutagenesis, could allow a much more comprehensive study of electrostatic vs. geometric effects on protein disulfide bond stability.

While there are still problems to be solved with roGFP indicators, as ratiometric fluorescence reporters with high spatial and temporal resolution they remain extremely valuable tools for the study of intracellular redox events.



## BIBLIOGRAPHY

- Aslund, F., and Beckwith, J. 1999. The thioredoxin superfamily: redundancy, specificity and gray-area genomics. *Journal of Bacteriology* **181**: 1375-1379.
- Barford, D. 2004. The role of cysteine residues as redox-sensitive regulatory switches. *Current Opinion in Structural Biology* **14**: 679-686.
- Barondeau, D.P., Kassmann, C.J., Tainer, J.A., and Getzoff, E.D. 2002. Structural chemistry of a green fluorescent protein Zn biosensor. *J Am Chem Soc* **124**: 3522-3524.
- Biteau, B., Labarre, J., and Toledano, M.B. 2003. ATP-dependent reduction of cysteine-sulphinic acid by *S. cerevisiae* sulphiredoxin. *Nature* **425**: 980-984.
- Brejc, K., Sixma, T.K., Kitts, P.A., Kain, S.R., Tsien, R.Y., Ormo, M., and Remington, S.J. 1997. Structural basis for dual excitation and photoisomerization of the *Aequorea victoria* green fluorescent protein. *Proceedings of the National Academy of Sciences of the U.S.A.* **94**: 2306-2311.
- Burns, J.A., and Whitesides, G.M. 1990. Predicting the stability of cyclic disulfides by molecular modeling: "effective concentrations" in thiol-disulfide interchange and the design of strongly reducing dithiols. *J Am Chem Soc* **112**: 6296-6303.
- Cadwell, R.C., and Joyce, G.F. 1994. Mutagenic PCR. *PCR Methods Appl* **3**: S136-140.
- Camps, M., Naukkarinen, J., Johnson, B.P., and Loeb, L.A. 2003. Targeted gene evolution in *Escherichia coli* using a highly error-prone DNA polymerase I. *Proceedings of the National Academy of Sciences of the U.S.A.* **100**: 9727-9732.

- Chattoraj, M., King, B.A., Bublit, G.U., and Boxer, S.G. 1996. Ultra-fast excited state dynamics in green fluorescent protein: multiple states and proton transfer. *Proceedings of the National Academy of Sciences of the U.S.A.* **93**: 8362-8367.
- Chesney, J.A., Eaton, J.W., and Mahoney, J.R. 1996. Bacterial glutathione: a sacrificial defense against chlorine compounds. *Journal of Bacteriology* **178**: 2131-2135.
- Chivers, P.T., Prehoda, K.E., and Raines, R.T. 1997. The CXXC motif: a rheostat in the active site. *Biochemistry* **36**: 4061-4066.
- Choi, H.-J., Kang, S.W., Yang, C.-H., Rhee, S.G., and Ryu, S.-E. 1998. Crystal structure of a novel human peroxidase enzyme at 2.0 Å resolution. *Nat Struct Biol* **5**: 400-406.
- Creighton, T.E. 1975. Interactions between cysteine residues as probes of protein conformation: the disulfide bond between Cys-14 and Cys-38 of the pancreatic trypsin inhibitor. *J Mol Biol* **96**: 767-776.
- DeLano, W.L. 2002. The PyMOL Molecular Graphics System. *on World Wide Web* <http://www.pymol.org>.
- Delaunay, A., Pflieger, D., Barrault, M.-B., Vinh, J., and Toledano, M.B. 2002. A thiol peroxidase is an H<sub>2</sub>O<sub>2</sub> receptor and redox-transducer in gene activation. *Cell* **111**: 471-481.
- Dooley, C.T., Dore, T.M., Hanson, G.T., Jackson, W.C., Remington, S.J., and Tsein, R.Y. 2004. Imaging dynamic redox changes in mammalian cells with green fluorescent protein indicators. *J Biol Chem* **279**: 22284-22293.
- Dyson, H.J., Jeng, M.-F., Tennant, L.L., Slaby, I., Lindell, M., D.-S., C., Kuprin, S., and Holmgren, A. 1997. Effects of buried charged groups on cysteine thiol ionization and reactivity in *Escherichia coli* thioredoxin: structural and functional characterization of mutants of Asp 26 and Lys 57. *Biochemistry* **36**: 2622-2636.
- Elslinger, M.-A., Wachter, R.M., Hanson, G.T., Kallio, K., and Remington, S.J. 1999. Structural and spectral response of green fluorescent protein variants to changes in pH. *Biochemistry* **38**: 5296-5301.
- Finkel, T. 1998. Oxygen radicals and signaling. *Curr Opin Cell Biol* **10**: 248-253.

- Gane, P.J., Freedman, R.B., and Warwicker, J. 1995. A molecular model for the redox potential difference between thioredoxin and DsbA, based on electrostatics calculations. *J Mol Biol* **249**: 376-387.
- Glauser, D.A., Bourquin, F., Manieri, W., and Schurmann, P. 2004. Characterization of ferredoxin:thioredoxin reductase modified by site-directed mutagenesis. *J Biol Chem* **279**: 16662-16669.
- Grauschopf, U., Winther, J.R., Korber, P., Zander, T., Dallinger, P., and Bardwell, J.C. 1995. Why is DsbA such an oxidizing disulfide catalyst? *Cell* **83**: 947-955.
- Griesbeck, O. 2004. Fluorescent proteins as sensors for cellular functions. *Current Opinion in Neurobiology* **14**: 636-641.
- Grynkiewicz, G., Poenie, M., and Tsien, R.Y. 1985. A new generation of Ca<sup>2+</sup> indicators with greatly improved fluorescence properties. *J Biol Chem* **260**: 3440-3450.
- Hanson, G.T., Aggeler, R., Oglesbee, D., Cannon, M., Capaldi, R.A., Tsien, R.Y., and Remington, S.J. 2004. Investigating mitochondrial redox potential with redox-sensitive green fluorescent protein indicators. *J Biol Chem* **279**: 13044-13053.
- Hanson, G.T., McAnaney, T.B., Park, E.S., Rendell, M.E.P., Yarbrough, D.K., Chu, S., Xi, L., Boxer, S.G., Montrose, M.H., and Remington, S.J. 2002. Green fluorescent protein variants as ratiometric dual emission pH sensors. 1. Structural characterization and preliminary application. *Biochemistry* **41**: 15477-15488.
- Heim, R., Prasher, D.C., and Tsien, R.Y. 1994. Wavelength mutations and posttranslational autooxidation of green fluorescent protein. *Proceedings of the National Academy of Sciences of the U.S.A.* **91**: 12501-12504.
- Hofmann, B., Hecht, H.-J., and Flohe, L. 2002. Peroxiredoxins. *Biol Chem* **383**: 347-364.
- Hogg, P.J. 2003. Disulfide bonds as switches for protein function. *Trends Biochem Sci* **28**: 210-214.
- Hwang, C., Sinskey, A.J., and Lodish, H.F. 1992. Oxidized redox state of glutathione in the endoplasmic reticulum. *Science* **257**: 1496-1502.
- Jares-Erijman, E.A., and Jovin, T.M. 2003. FRET imaging. *Nature Biotechnology* **21**: 1387-1395.

- Jayaraman, S., Haggie, P., Wachter, R.M., Remington, S.J., and Verkman, A.S. 2000. Mechanism and cellular applications of a green fluorescent protein-based halide sensor. *J Biol Chem* **275**: 6047-6050.
- Jones, T.A., Zou, J.Y., Cowan, S.W., and Kjeldgaard, M. 1991. Improved methods for the building of protein models in electron density maps and the location of errors in these models. *Acta Crystallogr A* **47**: 110-119.
- Katz, B.A., and Kossiakoff, A. 1986. The crystallographically determined structures of atypical strained disulfides engineered into subtilisin. *J Biol Chem* **261**: 15480-15485.
- Kissinger, C.R., Gehlhaar, D.K., and Fogel, D.B. 1999. Rapid automated molecular replacement by evolutionary search. *Acta Crystallographica* **55**: 484-491.
- Kneen, M., J., F., Li, Y., and Verkman, A.S. 1998. Green fluorescent protein as a noninvasive intracellular pH indicator. *Biophys J* **74**: 1591-1599.
- Labas, Y.A., Gurskaya, N.G., Yanushevich, Y.G., Fradkov, A.F., Lukyanov, K.A., Lukyanov, S.A., and Matz, M.V. 2002. Diversity and evolution of the green fluorescent protein family. *Proceedings of the National Academy of Sciences of the U.S.A.* **99**: 4256-4261.
- Lees, W.J., and Whitesides, G.M. 1993. Equilibrium constants for thiol-disulfide interchange reactions: a coherent, corrected set. *Journal of Organic Chemistry* **58**: 642-647.
- Lindley, H. 1960. A study of the kinetics of the reaction between thiol compounds and chloroacetamide. *Biochem J* **74**: 577-584.
- Llopis, J., J.M., M., Miyawaki, A., Farquhar, M.G., and Tsien, R.Y. 1998. Measurement of cytosolic, mitochondrial, and Golgi pH in single living cells with green fluorescent proteins. *Proceedings of the National Academy of Sciences of the U.S.A.* **95**: 6803-6808.
- Lowther, W.T., Weissbach, H., Etienne, F., Brot, N., and Matthews, B.W. 2002. The mirrored methionine sulfoxide reductases of *Neisseria gonorrhoeae* pilB. *Nat Struct Biol* **9**: 348-352.
- Martin, J.L. 1995. Thioredoxin--a fold for all reasons. *Structure* **3**: 245-250.
- Martin, J.L., Bardwell, J.C., and Kuriyan, J. 1993. Crystal structure of the DsbA protein required for disulfide bond formation in vivo. *Nature* **365**: 464-468.

- Matthias, L.J., Yam, P.T.W., Jiang, X.-M., Vandegraaff, N., Li, P., Poulos, P., Donoghue, N., and Hogg, P.J. 2002. Disulfide exchange in domain 2 of CD4 is required for entry of HIV-1. *Nature Immunology* **3**: 727-732.
- Matz, M.V., Fradkov, A.F., Labas, Y.A., Savitsky, A.P., Zaraisky, A.G., Markelov, M.L., and Lukyanov, S.A. 1999. Fluorescent proteins from nonbioluminescent Anthozoa species. *Nature Biotechnology* **17**: 969-973.
- Miesenbock, G., De Angelis, D.A., and Rothman, J.E. 1998. Visualizing secretion and synaptic transmission with pH-sensitive green fluorescent proteins. *Nature* **394**: 192-195.
- Mills, C.E. 2004. Bioluminescence of Aequorea, a hydromedusa. *on World Wide Web* <http://faculty.washington.edu/cemills/Aequorea.html>.
- Moutevelis, E., and Warwicker, J. 2004. Prediction of pKa and redox properties in the thioredoxin superfamily. *Protein Science* **13**: 2744-2752.
- Nagai, T., Sawano, A., Park, E.S., and Miyawaki, A. 2001. Circularly permuted green fluorescent proteins engineered to sense Ca<sup>2+</sup>. *Proceedings of the National Academy of Sciences of the U.S.A.* **98**: 3197-3202.
- Nelson, J.W., and Creighton, T.E. 1994. Reactivity and ionization of the active site cysteine residues of DsbA, a protein required for disulfide bond formation in vivo. *Biochemistry* **33**: 5974-5983.
- Ormo, M., Cubitt, A.B., Kallio, K., Gross, L.A., Tsien, R.Y., and Remington, S.J. 1996. Crystal structure of the Aequorea victoria green fluorescent protein. *Science* **273**: 1392-1395.
- Ostergaard, H., Henriksen, A., Hansen, F.G., and Winther, J.R. 2001. Shedding light on disulfide bond formation: engineering a redox switch in green fluorescent protein. *EMBO J* **20**: 5853-5862.
- Otwinowski, Z., and Minor, W. 1997. Processing of x-ray diffraction data collected in oscillation mode. *Methods Enzymol* **276**: 307-326.
- Paget, M.S., and Buttner, M.J. 2003. Thiol-based regulatory switches. *Annu Rev Genet* **37**: 91-121.
- Patterson, G.H., Knobel, S.M., Sharif, W.D., Kain, S.R., and Piston, D.W. 1997. Use of the green fluorescent protein and its mutants in quantitative fluorescence microscopy. *Biophys J* **73**: 2782-2790.

- Prasher, D.C., Eckenrode, V.K., Ward, W.W., Prendergast, F.G., and Cormier, M.J. 1992. Primary structure of the *Aequorea victoria* green-fluorescent protein. *Gene* **111**: 229-133.
- Ramos, C.H.I., and Baldwin, R.L. 2002. Sulfate anion stabilization of native ribonuclease A both by anion binding and by the Hofmeister effect. *Protein Science* **11**: 1771-1778.
- Rhee, S.G. 1999. Redox signaling: hydrogen peroxide as intracellular messenger. *Experimental and Molecular Medicine* **31**: 53-59.
- Rhee, S.G., Bae, Y.S., Lee, S.-R., and Kwon, J. 2000. Hydrogen peroxide: a key messenger that modulates protein phosphorylation through cysteine oxidation. *Sci STKE* **53**: PE1.
- Rhee, S.G., Chang, T.-S., Bae, Y.S., Lee, S.-R., and Kang, S.W. 2003. Cellular regulation by hydrogen peroxide. *J Am Soc Nephrol* **14**: S211-S215.
- Rhee, S.G., Kang, S.W., Chang, T.-S., Jeong, W., and Kim, K. 2001. Peroxiredoxin, a novel family of peroxidases. *IUBMB Life* **52**: 35-41.
- Rocchia, W., Alexov, E., and Honig, B. 2001. Extending the applicability of the nonlinear Poisson-Boltzmann equation: multiple dielectric constants and multivalent ions. *J Phys Chem B* **105**: 6507-6514.
- Rocchia, W., Sridharan, S., Nicholls, A., Alexov, E., Chiabrera, A., and Honig, B. 2002. Rapid grid-based construction of the molecular surface for both molecules and geometric objects: applications to the finite difference Poisson-Boltzmann method. *J Comp Chem* **23**: 128-137.
- Rossignol, R., Gilkerson, R., Aggeler, R., Yamagata, K., Remington, S.J., and Capaldi, R.A. 2004. Energy substrate modulates mitochondrial structure and oxidative capacity in cancer cells. *Cancer Research* **64**: 985-993.
- Salmeen, A., Andersen, J.N., Myers, M.P., Meng, T.C., Hinks, J.A., Tonks, N.K., and Barford, D. 2003. Redox regulation of protein tyrosine phosphatase 1B involves a sulphenyl-amide intermediate. *Nature* **423**: 769-773.
- Sawano, A., and Miyawaki, A. 2000. Directed evolution of green fluorescent protein by a new versatile PCR strategy for site-directed and semi-random mutagenesis. *Nucleic Acids Res* **28**: e78.

- Schafer, F.Q., and Buettner, G.R. 2001. Redox environment of the cell as viewed through the redox state of the glutathione disulfide/glutathione couple. *Free Radical Biology & Medicine* **30**: 1191-1212.
- Shimomura, O., and Johnson, F.H. 1973. Chemical nature of light emitter in bioluminescence of aequorin. *Tetrahedron Letters* **31**: 2963-2966.
- Srinivasan, N., Sowdhamini, R., Ramakrishnan, C., and Balaram, P. 1990. Conformations of disulfide bridges in proteins. *Int J Peptide Protein Res* **36**: 147-155.
- Szajewski, R.P., and Whitesides, G.M. 1980. Rate constants and equilibrium constants for thiol-disulfide interchange reactions involving oxidized glutathione. *J Am Chem Soc* **102**: 2011-2015.
- Tanford, C., and Kirkwood, J.G. 1957. Theory of protein titration curves. I. General equations for impenetrable spheres. *J Am Chem Soc* **79**: 5333-5339.
- Tronrud, D.E., Ten Eyck, L.F., and Matthews, B.W. 1987. An efficient general-purpose least-squares refinement program for macromolecular structures. *Acta Crystallogr A* **43**: 489-501.
- Tsien, R.Y. 1998. The green fluorescent protein. *Annu Rev Biochem* **67**: 509-544.
- van Montfort, R.L., Congreve, M., Tisi, D., Carr, R., and Jhoti, H. 2003. Oxidation state of the active-site cysteine in protein tyrosine phosphatase 1B. *Nature* **423**: 773-777.
- Voet, D., Voet, J.G., and Pratt, C.W. 1999. *Fundamentals of Biochemistry*. John Wiley & Sons, Inc., New York.
- Wachter, R.M., King, B.A., Heim, R., Kallio, K., Tsien, R.Y., Boxer, S.G., and Remington, S.J. 1997. Crystal structure and photodynamic behavior of the blue emission variant Y66H/Y145F of green fluorescent protein. *Biochemistry* **36**: 9759-9765.
- Wachter, R.M., and Remington, S.J. 1999. Sensitivity of the yellow variant of green fluorescent protein to halides and nitrate. *Current Biology* **9**: R628-R629.
- Wachter, R.M., Yarbrough, D., Kallio, K., and Remington, S.J. 2000. Crystallographic and energetic analysis of binding of selected anions to the yellow variants of green fluorescent protein. *J Mol Biol* **301**: 157-171.

- Weber, G., and Teale, F.W.J. 1957. Determination of the absolute quantum yield of fluorescent solutions. *Trans Faraday Soc* **53**: 646-655.
- Wells, J.A., and Powers, D.B. 1986. *In vivo* formation and stability of engineered disulfide bonds in subtilisin. *J Biol Chem* **261**: 6564-6570.
- Yang, A.-S., Gunner, M.R., Sampogna, R., Sharp, K., and Honig, B. 1993. On the calculation of pKas in proteins. *Proteins* **15**: 252-265.
- Yang, F., Moss, L.G., and Phillips, G.N.J. 1996. The molecular structure of green fluorescent protein. *Nature Biotechnology* **14**: 1246-1251.
- Zhang, J., Campbell, R.E., Ying, A.Y., and Tsien, R.Y. 2002. Creating new fluorescent probes for cell biology. *Nature Reviews Molecular Cell Biology* **3**: 906-918.
- Zhang, X., and Matthews, B.W. 1995. EdPDB: A multi-functional tool for protein structure analysis. *J Appl Cryst* **28**: 624-630.
- Zhang, Z.Y., and Dixon, J.E. 1993. Active site labeling of the *Yersinia* protein tyrosine phosphatase: the determination of the pK<sub>a</sub> of the active site cysteine and the function of the conserved histidine 402. *Biochemistry* **32**: 9340-9345.